

Journal of Research of the National Bureau of Standards

Volume 89

Number 5

September-October

Evaluation of Some High-Temperature Platinum Resistance Thermometers.
J. P. Evans 349

Automated High-Temperature PVT Apparatus With Data for Propane.
G. C. Straty and A. M. F. Palavra 375

Radio Propagation in a Coal Seam and the Inverse Problem.
D. A. Hill 385

A Report on the National Bureau of Standards pH Standards.
Y. C. Wu, W. F. Koch, and G. Marinenko 395

Published Papers of the National Bureau of Standards 401

ISSN 0160-1741

Library of Congress Catalog Card No.: 63-37059

The Journal of Research of the National Bureau of Standards features advances in measurement methodology and analyses consistent with the NBS responsibility as the nation's measurement science laboratory. It includes reports on instrumentation for making accurate and precise measurements in fields of physical science and engineering, as well as the mathematical models of phenomena which enable the predictive determination of information in regions where measurements may be absent. Papers on critical data, calibration techniques, quality assurance programs, and well characterized reference materials reflect NBS programs in these areas. Special issues of the Journal are devoted to invited papers in a particular field of measurement science. Survey articles appear periodically on topics related to the Bureau's technical and scientific programs. As a special service to subscribers each issue contains complete citations to all recent NBS publications in NBS and non-NBS media.

David T. Goldman, Editor

Executive Editors
Donald R. Johnson
(Natl. Measurement Lab.)
John W. Lyons
(Natl. Engineering Lab.)

Board of Editors

John W. Cooper (Physics) Howard J. M. Hanley
Sharon G. Lias (Chemistry) (Boulder Laboratory)
Donald G. Eitzen (Engineering) John W. Cahn (Materials)

Issued six times a year. Annual subscriptions: domestic \$17.00; foreign \$21.25. Single copy, \$3.00 domestic; \$3.75 foreign.

United States Government Printing Office, Washington: 1984
Order all publications from the Superintendent of Documents
U.S. Government Printing Office, Washington, DC 20402

The Secretary of Commerce has determined that the publication of the periodical is necessary in the transaction of the public business required by law of this Department. Use of funds for printing this periodical has been approved by the Director of the Office of Management and Budget through April 1, 1985.

Evaluation of Some High-Temperature Platinum Resistance Thermometers

J. P. Evans

National Bureau of Standards, Gaithersburg, MD 20899

Accepted: July 17, 1984

Two sets of high-temperature platinum resistance thermometers of different design have been tested in the temperature range 0 to 1100 °C. One set was constructed at the National Institute of Metrology, in the People's Republic of China, and the other at the National Bureau of Standards. The results of the tests provide information on long- and short-time thermometer stability, and on other characteristics such as temperature coefficient, immersion, self-heating effect, electrical leakage, and durability. The results also show that the behavior of the two sets is similar enough to allow them to be considered as a single set of thermometers, and that the sets perform as well as, or better than, other sets of thermometers tested earlier. It is expected that this information will aid in the evaluation of the high-temperature platinum resistance thermometer as an interpolating instrument for a practical temperature scale up to the gold point.

Key words: electrical guarding; high temperature; immersion; performance; platinum resistance thermometer; practical temperature scale; self-heating effect; stability.

1. Introduction

The high-temperature platinum resistance thermometer has long been advocated as a standard interpolating instrument for a practical temperature scale up to the gold point, in place of the standard thermocouple. Acceptance of the resistance thermometer for this purpose is likely to come only when sufficient information is available for careful evaluation of thermometer characteristics and performance as they relate to the definition of a practical temperature scale.

The experiments and results reported here are intended to provide some of the needed information on the behavior of high-temperature resistance thermometers; specifically on the following characteristics:

- 1) Long-time stability at high temperature
- 2) Short-time stability upon temperature cycling
- 3) Temperature coefficient of resistance
- 4) Immersion characteristics

- 5) Heating effect of measuring current
- 6) Electrical leakage of thermometer supporting parts
- 7) Thermometer durability
- 8) Agreement among thermometers of derived temperature values.

Another purpose of this paper is to describe some experimental procedures that have proved useful in evaluating thermometer performance. The procedures require little in the way of apparatus beyond what is needed for routine thermometer measurement, calibration, and conditioning.

A third purpose of this paper is to report on the behavior of two sets of high-temperature platinum resistance thermometers from different sources and of different design. One set was constructed at the National Institute of Metrology (NIM), Beijing, People's Republic of China; the thermometers were lent to the National Bureau of Standards (NBS) for testing. The other set was constructed at the NBS. Both types of thermometers have been described in the literature [1–6].¹

About the Author: J. P. Evans is a physicist in the Temperature and Pressure Division of NBS' Center for Basic Standards.

¹Figures in brackets indicate the literature references at the end of this paper.

2. General Methods and Equipment

The general methods and equipment that were used to test the thermometers also have been described [3]. The descriptions are repeated in the following sections for convenience and completeness; they have been updated, where necessary, to apply to the lower resistance thermometers that were used in the present experiments.

2.1 Thermometer Heat-treating Furnace

Thermometers are heat-treated in a vertical annealing furnace capable of reaching 1100 °C. The furnace contains a relatively short cylindrical electrical heater near the center that heats only the resistor and a short section (a few centimeters) of adjacent leads to the selected heating temperature. During heat treatment, the thermometers are inserted into closed-end, silica-glass furnace wells, with the resistors situated in the hottest region of the furnace. The space between the wells and the heater contains only air. Six thermometers can be heated at one time.

The furnace is controlled by a Type B thermocouple (Pt–30%Rh/Pt–6%Rh), and it is monitored by a Type S thermocouple (Pt–10%Rh/Pt). A calibrated test thermometer can also be used for monitoring. The control system is capable of maintaining the furnace at a desired temperature within about 2 K, and is also capable of controlling furnace cooling at a uniform rate of 80 K/h.

For heat treatment, the thermometer sheaths are first thoroughly cleaned by appropriate means (e.g., acids or solvents) to remove dirt and fingerprints. The thermometers are then inserted into the furnace described above, which has been set to control at the desired temperature. At the end of the heating period, the control system is set to reduce the furnace temperature at the programmed rate of 80 K/h so as to avoid quenching in lattice-site vacancies [7]. When the furnace temperature reaches about 520 °C, the thermometers are removed. This procedure avoids the effects of the platinum oxidation that could occur if thermometers were allowed to cool slowly to room temperature [8].

2.2 Fixed Points

The triple point of water is realized in a conventional sealed glass cell. The ice mantle is prepared using a special immersion cooler [9] at least 24 h before measurements are to be made, and the cell is stored in an ice bath. During use, the ice mantle is free to rotate within the cell, the annulus between the cell well and the thermometer contains an aluminum bushing and water, and

the cell is shielded from ambient radiation. When a thermometer is fully immersed in a triple-point cell, the bottom tip of its sheath is about 275 mm below the surface of the liquid water.

The metal freezing points are also realized in sealed cells. The high-purity metal is contained in a graphite crucible with a re-entrant graphite well, and the graphite is surrounded by a sealed glass envelope. Before the cell is sealed, it is evacuated and filled with enough pure argon to provide a pressure of 1 atm at the freezing point. The cell is similar to the type 1 cell described by Furukawa [10].

The freezing points of all the cells have been found to be sufficiently constant during a single freeze, and sufficiently reproducible from freeze to freeze, to serve the requirements of thermometer testing. The tin, zinc, and silver cells contain Standard Reference Material metals (SRM 741, 740, and 748, respectively) obtained from the NBS Office of Standard Reference Materials. The materials are known to be of high purity (less than 1 ppm total impurity content), and the freezing points of the tin and zinc cells have been established to be well within 1 mK of the freezing points maintained in the NBS Thermometer Calibration Laboratory. The aluminum cell contains metal obtained from a commercial supplier who reported the impurity content to be less than 1 ppm. The gold cell contains a sample used in an earlier cell [11]. From the results of tests conducted with the earlier cell, including a comparison with the freezing point of a sample of known high purity, the freezing point of the present cell is believed to be within about 10 mK of the gold point. All of the cells except the gold cell provide a depth of thermometer immersion, from the top of the liquid metal to the inside bottom of the graphite well, of about 17 cm. The immersion in the gold cell is about 15 cm.

The metal freezing-point cells are heated in vertical electrical furnaces different from the annealing furnace. These furnaces are similar to those described earlier [11], but the present furnaces employ only a single long heating zone, and temperature equalization is achieved with aluminum cylinders or heat pipes. The tin and zinc cells are encased in aluminum cylinders located near the center of the zone; the cylinder walls are about 2 cm thick. The aluminum, silver, and gold cells are centered in coaxial heat pipes, about 10 cm o.d., 5 cm i.d., and 45 cm long, made of Inconel and containing sodium as the working fluid. The cylinders and heat pipes serve to establish for the cells a uniform temperature environment that is maintained about 1 K below the freezing point by control systems during freezing.

The metal freezing points are established by induced freezing. Except for tin, the molten metals are allowed

to cool slowly through the supercooled region until they recalesce. A solid mantle of metal is then induced on the cell well by inserting a cool rod. For tin, the freeze is induced in the supercooled metal by blowing air down the cell well, recalescence being detected by a thermocouple wrapped around the glass envelope.

Test thermometers are first preheated for about 5 min in the furnace just above the freezing point cell, and then measurements at full thermometer immersion are started after the system has come to thermal equilibrium. Except for special tests, the measurement process takes about 30 min, and at least five thermometers can be tested in a single freeze at the tin, zinc, and aluminum points. The gold and silver are remelted after each thermometer test. After testing at the gold, silver, or aluminum points, thermometers are placed in the annealing furnace, held at a temperature near the fixed point for 30 minutes, and then cooled at the programmed rate to 520 °C to anneal out lattice site defects. Following this, and also after tin- and zinc-point measurements, the resistance at the triple point of water is determined.

2.3 Electrical Measurements

Measurements of thermometer resistance are made with an automatic self-balancing bridge [12], and a computer is used to control the operation of the bridge and record the data. The bridge utilizes square-wave excitation, normally at 30 Hz, though 15 Hz can be selected. It also has provision for selecting thermometer measuring current of 1, 2, 4, or 8 mA and one of four resistor input channels. It can resolve resistance to less than 1 micro-ohm with a linearity of 1 part in 10^7 .

Thermometer resistance is determined from a sequence of measurements of both the thermometer and a relatively stable (20 micro-ohm per year drift) 10-ohm standard resistor located in a temperature-controlled oil bath. When a thermometer, carrying a normal measuring current of 4 mA, has come to thermal equilibrium in a fixed-point cell, 10 readings of its resistance are recorded. The system then switches to the standard resistor and records 10 readings at the same current. Immediately thereafter, the thermometer is reconnected to the bridge and the measuring current is doubled. When the thermometer has come to thermal equilibrium at this higher current (a period of 3 min is usually allowed), additional sets of 10 readings are recorded for the thermometer and standard resistor. The entire process takes about 7 min. From these data, a mean value of the ratio of thermometer resistance to standard-resistor resistance, extrapolated to zero measuring current, is computed and stored. The computer also calculates the heating effect of the normal measuring current, and the

estimated standard deviation of the computed mean ratio value. This standard deviation seldom exceeds the equivalent of 0.2 micro-ohm.

3. Thermometers

The thermometers used in the experiments were in some ways similar to other high-temperature platinum resistance thermometers that have been described in recent years [3,5,11]. The temperature sensing resistors were 1 to 3 cm long and about 0.5 cm in diameter, they were connected to four platinum leads, and they were sealed in long (70–80 cm) silica-glass tubes. Thermometer resistance at 0 °C was small—less than 1 ohm.

In other ways the thermometers were novel. The resistors in the NIM thermometers were of the single-layer, bifilar helix design, but the support for the resistor wire consisted of a single notched silica-glass blade, rather than the customary cross. The NBS thermometers employed newly-designed “toroidal” resistors and guarded leads. Detailed features of the thermometers are presented in tables 1 and 2.

The NIM thermometers had been stabilized by heat treatment, as indicated in table 2, before they were transported to NBS. Properties of the thermometers measured at the NIM during the stabilization are shown in figure 1. Upon their arrival at the NBS the four NIM thermometers were inspected. It was observed that three thermometers (18227, 18236, 18237) had bent sheaths, and that in two of the thermometers (18227 and

Table 1. General features of thermometers.

	NIM	NBS
Overall length		
(including header)	805 mm	885 mm
Header length	85 mm	125 mm
External tube length	720 mm	760 mm
Nominal tube diameter	7 mm	7 mm
Header diameter	20 mm	19 mm
Resistor type	Single layer helix	Toroidal (straight wire)
Resistor former	Notched silica blade	Notched-end silica tube
Former length	40 mm	15 mm
Resistor coil length	30 mm	10 mm
Resistor wire diameter	0.4 mm	0.25 mm
Nominal resistance at 0 °C	0.25 ohm	0.37 ohm
Lead insulator type	Silica tube and disk	Long silica tubes with internal guard
Lead wire diameter	0.3 mm	0.25 mm
Length of roughened sheath surface	350 mm	500 mm
External connection	Permanent copper lead wire cable	Separable five-pin connector on header

Table 2. Features of individual thermometers.

Thermometer number	Nominal resistance at 0 °C, ohm	Initial stabilization, h at 1100 °C	Alpha coefficient, α , at beginning of test, $\times 10^6, K^{-1}$	Distance in mm, bottom of former to bottom of sheath at room temperature
NIM thermometers				
80179	0.244	350	3927.1	1.0
18227	0.260	350	3926.9	0.5
18236	0.257	350	3926.8	0
18237	0.263	500	3926.8	1.5
NBS thermometers				
8202	0.373	400	3926.9	7.5
8204	0.361	400	3927.0	7.0
8205	0.378	400	3926.8	7.5

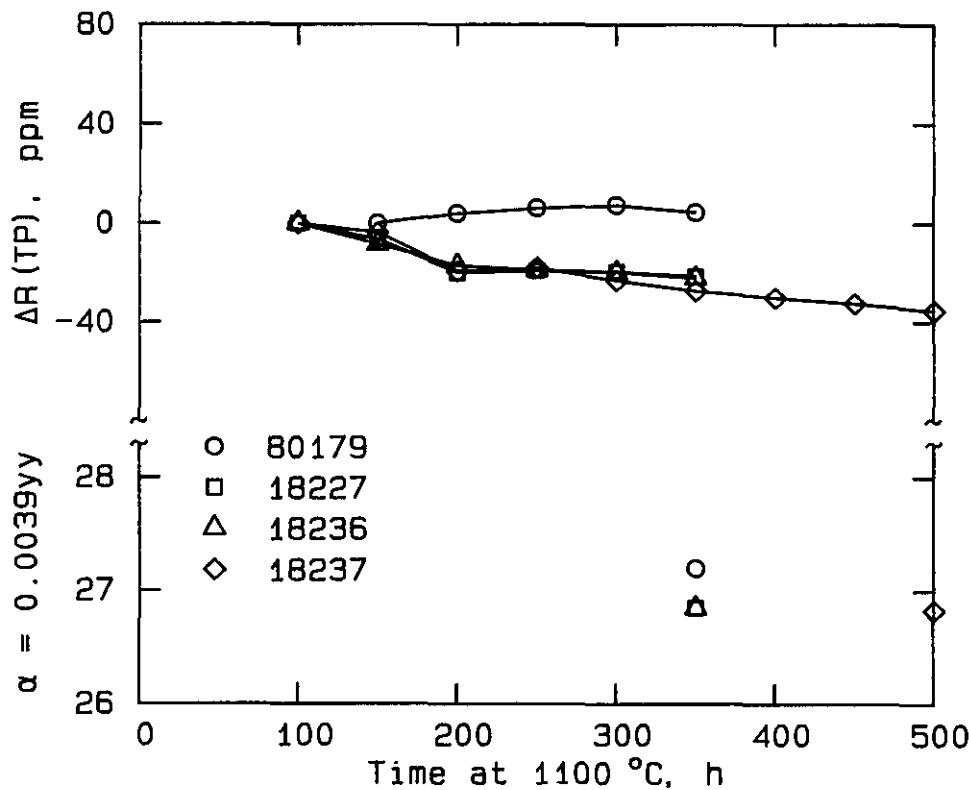


Figure 1—Change in characteristics of NIM thermometers during stabilization. The measurements were made at the National Institute of Metrology, Beijing. Both the relative change in thermometer resistance at the triple point of water (parts in 10^6 , ppm) and the alpha coefficient, α , are shown.

18236), the resistor support blade was bent. It was believed that these minor defects would not introduce unwanted biases into the experiments, so all four thermometers were prepared for testing by annealing them for 30 min at or near the gold point, and then slow-cooling them to about 520 °C.

The NBS thermometers had also been stabilized by heat treatment, as indicated in table 2 and figure 2. One of the four thermometers originally made for the investigation (8203) failed during the stabilization process because of internal lead separation. It therefore could not be included in any of the experiments.

4. Experimental Procedures and Results

Unless otherwise indicated, the general methods and equipment described above were used throughout the experiments. The internal guard of the guarded lead thermometers was connected to the bridge guard circuit during measurement [13], except for special tests. All experimental results are reported in the appendix tables. The values of resistance in the tables are given by

$$R = 10 \times R(\text{th}) / R(\text{sr}), \quad (1)$$

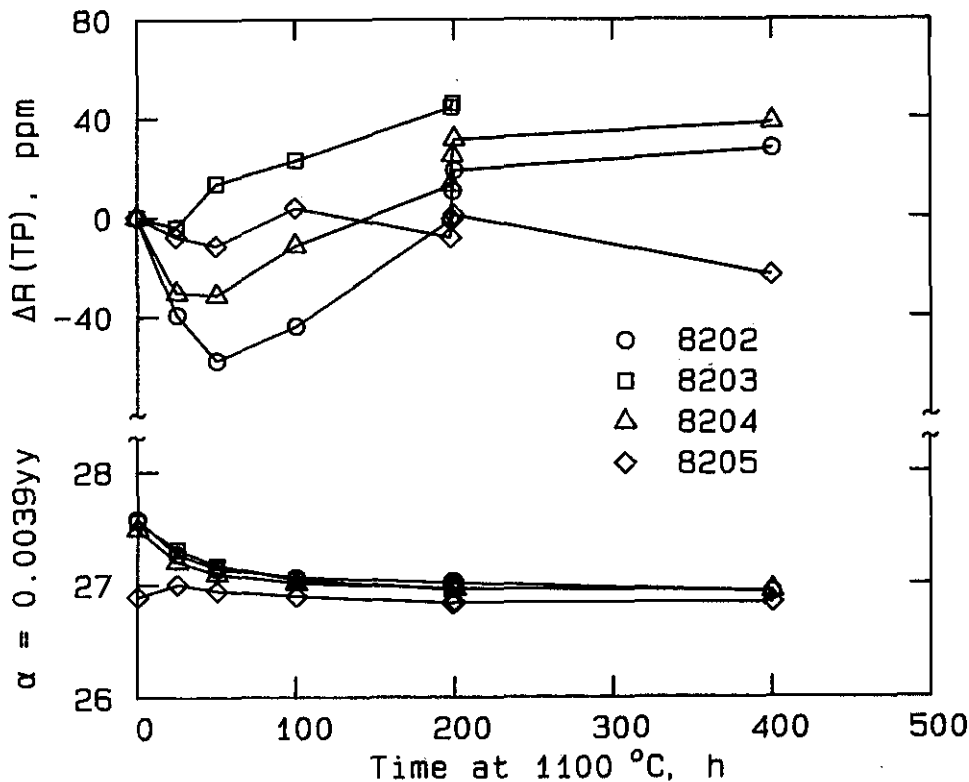


Figure 2—Change in characteristics of NBS thermometers during stabilization. Both the relative change in thermometer resistance at the triple point of water (parts in 10^6 , ppm) and the alpha coefficient, α , are shown.

where $R(th)$ is the value of the thermometer and $R(sr)$ is the value of the standard resistor, as measured by the bridge. The factor 10 in eq (1) is the nominal resistance of the standard resistor; it is included so that R is approximately in ohms. If the factor were to be replaced by the actual value of the standard resistor in absolute ohms, then R would also be in absolute ohms. This was not considered necessary for the present investigation because all results were derived from ratios of R values. In the time required to obtain the values of R for a single ratio, the standard resistor did not change significantly.

The first experiment consisted of two runs (series of measurements of thermometer resistance at fixed points) with an intervening exposure of the thermometers to high temperature. In the first run, the resistance of a thermometer was determined at thermometric fixed points in the sequence TP, AU, TP, AG, TP, AL, TP, ZN, TP, SN, TP, where TP designates the triple point of water and AU, AG, AL, ZN, SN designate the freezing points of gold, silver, aluminum, zinc, and tin, respectively. Three or four thermometers were measured in a single freeze at the tin, zinc, and aluminum points, but at the gold and silver points, separate freezes were used for each thermometer. The measurements were made with the thermometer fully immersed in the freezing-point cells and in the triple-point cell. Thermometer resistance was determined both with the nor-

mal measuring current and with twice the normal current; the value of resistance for zero power dissipation was calculated from these two determinations. The thermometer was then heated in a vertical position at 1100 °C for 100 h and cooled slowly as described above (sec. 2.1), and the measurement sequence was repeated for the second run. The results are given in tables A1a-g of the appendix.

The second experiment was conducted at the silver point. A "mesh" made of 0.25 mm diameter platinum wire was placed around the sheath of a thermometer before it was inserted into the silver freezing-point cell. Upon insertion, the mesh was situated in the small annulus between the silica-glass sheath of the thermometer and the silica-glass cell guide tube and cell well, thus preventing direct contact between the sheath and the guide tube and well. The mesh extended all the way from the bottom of the thermometer to the top of the cell guide tube at room temperature, where it was connected electrically to the bridge guard circuit, forming an external electrical thermometer guard. Thermometer resistance determinations were made, with the normal measuring current, at 5 min intervals as the silver was allowed to freeze slowly. From time to time the connection between the bridge guard circuit and the thermometer guards was changed, or the guard circuit was disconnected completely. Results for all thermometers

except No. 18227 (NIM) are given in tables A2a-f of the appendix.

Thermometer No. 18227 was not tested in the second experiment because the slightly larger diameter of its sheath did not leave enough room in the cell well to accommodate the wire mesh. Similarly, the slightly smaller diameter of the gold-point cell well prevented the use of the external guard with any of the thermometers at the gold point.

In the third experiment the immersion characteristics of the thermometers were compared at the freezing point of zinc. The zinc point was chosen for this experiment because electrical leakage effects were negligible, and because it was easy to establish long periods of constant temperature. Only the normal measuring current was used; precise determination of variations in thermometer self-heating would have been obscured by the limited bridge resolution of the thermometers' low resistance. Measurements were made at 5 min intervals at various vertical stations (in cm) in the cell well. The results are given in tables A3a-b of the appendix. At station 0, the thermometer sheath was fully immersed in and resting on the bottom of the cell well.

5. Analysis of Data

5.1 First Experiment

The data obtained in the first experiment may be analyzed by deriving the resistance ratio at each fixed point from the resistance values given in tables A1a-g. The resistance ratio at a fixed point, designated by $W(\text{FP})$, is defined by

$$W(\text{FP}) = R(\text{FP})/R(0). \quad (2)$$

$R(\text{FP})$ is the resistance at the fixed point taken from the tables. $R(0)$ is the associated value of thermometer resistance at 0°C ; it is derived from the mean of the values of $R(\text{TP})$ immediately preceding and following $R(\text{FP})$ in the tables, taking into account a correction for the depth of immersion of the thermometer in the triple-point cell. The values of $W(\text{FP})$ are listed in table 3.

It is convenient to interpret resistance ratios and their differences in terms of temperature values. To do this,

Table 3. Resistance ratios at fixed points.^{1,2}

Run	$W(\text{AU})$	$W(\text{AG})$	$W(\text{AL})$	$W(\text{ZN})$	$W(\text{SN})$
RT no. 80179					
1	4.57174066	4.28647159	3.37604256	2.56895487	1.89283568
2	4.57168631	4.28642060	3.37600925	2.56893131	1.89282128
RT no. 18227					
1	4.57157254	4.28629894	3.37591813	2.56886467	1.89278068
2	4.57151496	4.28623733	3.37587016	2.56883989	1.89276336
RT no. 18236					
1	4.57148343	4.28625191	3.37588957	2.56884678	1.89277435
2	4.57147650	4.28622095	3.37585840	2.56882739	1.89275797
RT no. 18237					
1	4.57149741	4.28628074	3.37591249	2.56886121	1.89277637
2	4.57145197	4.28622217	3.37586485	2.56883266	1.89276204
RT no. 8202					
1	4.57150591	4.28624231	3.37592544	2.56888096	1.89279537
2	4.57147188	4.28622642	3.37590991	2.56887218	1.89279135
RT no. 8204					
1	4.57152289	4.28627237	3.37594233	2.56888153	1.89279772
2	4.57153108	4.28627577	3.37594331	2.56887922	1.89279320
RT no. 8205					
1	4.57137553	4.28617237	3.37587835	2.56884607	1.89277446
2	4.57136712	4.28614094	3.37586420	2.56884047	1.89277239

¹Values derived from resistance values given in tables A1a-g.

² $W(\text{FP}) = R(\text{FP})/R(0)$, where $R(0)$ is derived from the mean of the values of $R(\text{TP})$ before and after $R(\text{FP})$.

we define a simple "temperature scale" on which values of temperature (designated by t') lie close to values on ordinary scales. The resistance ratio of a thermometer is related to a value on the scale by

$$W(t') = 1 + At' + Bt'^2. \quad (3)$$

The coefficients A and B are determined from the values of $W(\text{SN})$ and $W(\text{ZN})$ in table 3 using the IPTS-68 assigned values of t' at the tin and zinc points, but taking into account corrections due to thermometer immersion. The values of A and B are listed in table 4, along with values of the coefficients alpha, α , and delta, δ , related to A and B by

$$\alpha = A + 100B; \quad \delta = -10^4 B / (A + 100B). \quad (4)$$

The values of t' calculated from the values of $W(\text{AL})$, $W(\text{AG})$, and $W(\text{AU})$ in table 3, using eq (3), represent values of temperature in the respective metal freezing point cells during freezing experiments, specifically at the mid-point of the resistor of a fully immersed ther-

mometer. The values obtained from runs 1 and 2 are listed in table 5.

Table 6 summarizes pertinent statistics of the values in table 5. The data are analyzed in various subsets and combinations of subsets as indicated. "Mean" is the arithmetic mean of the equally weighted values in the subset. "SD" is the estimate of the standard deviation of one value in the subset derived from the data in the subset. "Range" is the difference between the maximum and minimum values in the subset. All values are given in "degrees" on the "temperature scale"—close to degrees C or kelvins on ordinary scales.

Table 7 gives the temperature equivalents of the resistance ratio changes between run 1 and run 2. The temperature differences are estimated from

$$\Delta t = \Delta W / (dW/dt), \quad (5)$$

where $\Delta W = W(\text{run 2}) - W(\text{run 1})$, and $W(\text{run 1})$ is the value of $W(\text{FP})$ determined in run 1 at a fixed point, and $W(\text{run 2})$ is the value of $W(\text{FP})$ at the same fixed point determined during run 2, both taken from table 3. The derivative dW/dT , obtained by differentiating eq (3), is

Table 4. Calibration coefficients.^{1,2}

Run	A	B	α	δ
RT no. 80179				
1	3985.8728E-6 ³	-0.58756370E-6	3927.1164E-6	1.4961708
2	3985.8033E-6	-0.58753192E-6	3927.0502E-6	1.4961151
RT no. 18227				
1	3985.6083E-6	-0.58744562E-6	3926.8637E-6	1.4959664
2	3985.5143E-6	-0.58736232E-6	3926.7781E-6	1.4957869
RT no. 18236				
1	3985.6000E-6	-0.58752738E-6	3926.8472E-6	1.4961809
2	3985.4992E-6	-0.58739730E-6	3926.7594E-6	1.4958831
RT no. 18237				
1	3985.5769E-6	-0.58739055E-6	3926.8379E-6	1.4958360
2	3985.5229E-6	-0.58742386E-6	3926.7805E-6	1.4959427
RT no. 8202				
1	3985.7019E-6	-0.58757620E-6	3926.9443E-6	1.4962682
2	3985.6890E-6	-0.58759525E-6	3926.9295E-6	1.4963224
RT no. 8204				
1	3985.7229E-6	-0.58762304E-6	3926.9606E-6	1.4963813
2	3985.6862E-6	-0.58754853E-6	3926.9313E-6	1.4962027
RT no. 8205				
1	3985.6031E-6	-0.58753878E-6	3926.8492E-6	1.4962092
2	3985.5996E-6	-0.58756233E-6	3926.8434E-6	1.4962714

¹ $W(t') = 1 + At' + Bt'^2$.

² Coefficients derived from values of $W(\text{ZN})$ and $W(\text{SN})$ and IPTS-68 assigned values of $t'(\text{ZN})$ and $t'(\text{SN})$.

³ The notation E-6 signifies multiplication by 10^{-6} .

Table 5. Derived values of t' at AU, AG, and AL.^{1,2}

RT no.	t' (AU)		t' (AG)		t' (AL)	
	Run 1	Run 2	Run 1	Run 2	Run 1	Run 2
80179	1062.5201	1062.5141	960.5363	960.5315	660.4079	660.4075
18227	1062.5127	1062.4938	960.5266	960.5098	660.4075	660.4006
18236	1062.5171	1062.5004	960.5394	960.5204	660.4114	660.4048
18237	1062.4747	1062.4928	960.5130	960.5215	660.4047	660.4055
8202	1062.5059	1062.5063	960.5175	960.5225	660.4082	660.4086
8204	1062.5232	1062.5098	960.5361	960.5256	660.4155	660.4133
8205	1062.4812	1062.4892	960.5142	960.5120	660.4088	660.4083

¹ $W(t')=1+At'+Bt'^2$.

²Values of t' derived from values of $W(FP)$ in table 3 and values of the coefficients in table 4.

Table 6. Statistics of t' .¹

RT set		Run 1	Run 2	Combined runs
at gold point (Au)				
NIM	Mean	1062.5062	1062.5003	1062.5032
	SD ²	0.0212	0.0098	0.0156
	Range	0.0454	0.0213	0.0454
NBS	Mean	1062.5034	1062.5018	1062.5026
	SD	0.0211	0.0110	0.0151
	Range	0.0420	0.0206	0.0420
Com- bined Set	Mean	1062.5050	1062.5009	1062.5030
	SD	0.0194	0.0094	0.0148
	Range	0.0485	0.0249	0.0485
at silver point (AG)				
NIM	Mean	960.5288	960.5208	960.5248
	SD	0.0119	0.0089	0.0106
	Range	0.0264	0.0217	0.0296
NBS	Mean	960.5226	960.5200	960.5213
	SD	0.0118	0.0071	0.0088
	Range	0.0219	0.0136	0.0241
Com- bined set	Mean	960.5262	960.5205	960.5233
	SD	0.0113	0.0075	0.0097
	Range	0.0264	0.0217	0.0296
at aluminum point (AL)				
NIM	Mean	660.4079	660.4046	660.4062
	SD	0.0027	0.0029	0.0031
	Range	0.0057	0.0069	0.0108
NBS	Mean	660.4108	660.4101	660.4104
	SD	0.0041	0.0028	0.0031
	Range	0.0073	0.0050	0.0073
Com- bined set	Mean	660.4091	660.4069	660.4080
	SD	0.0034	0.0039	0.0037
	Range	0.0108	0.0127	0.0149

¹Statistics derived from values of t' in table 5.

²SD: estimate of standard deviation of one value in indicated set.

evaluated using the coefficients from table 4 and the mean value of t' at the fixed point given in table 6 or the value of t' assigned to the fixed point.

It is instructive to evaluate t' from the values of $W(AU)$, $W(AG)$, and $W(AL)$ determined in run 2 using the values of the coefficients determined in run 1. The results of this procedure are given in table 8; these values are to be compared with the original run 1 values in tables 5 and 6. It can be seen that the temperature differences are the same as the temperature equivalent changes shown in table 7. This is to be expected, since both evaluations are based on the same "calibration coefficients"; the changes are thus due only to the changes in $W(AU)$, $W(AG)$, and $W(AL)$ between the two runs. A comparison of the statistics in table 8 with those in table 6 show that upon prolonged heating at high temperature the thermometers may change, resulting in changes in temperature values and increases in standard deviation and range if the thermometers are not recalibrated. Table 8 also shows similar results using run 2 coefficients and run 1 resistance ratios.

The results of an analysis at the silver point using a different "temperature scale" formulation are given in table 9. In this case, t'' is defined in terms of a quadratic relation between $W(t'')$ and t'' , as in eq (3), but with the coefficients determined at the aluminum and gold points (and at 0 °C). The coefficients are determined from the values of $W(AL)$ and $W(AU)$ given in table 3; the values of t'' assigned to these points, $t''(AL)=660.408$ and $t''(AU)=1062.503$, are the means of the combined sets and runs at the aluminum and gold points given in table 6. The statistics in table 9 are analogous to the statistics for t' at the silver point given in table 6.

The value of $R(TP)$ was determined six times for each thermometer during each of the two runs, as indicated in tables A1a-g. Table 10 presents a summary of the changes that occurred in $R(TP)$. The numbers in the table give relative, or fractional, changes in parts per million (parts in 10^6). The "Range" for a thermometer is

Table 7. Temperature equivalent of resistance ratio changes.^{1,2}

RT no.	AU	AG	AL	ZN	SN
80179	-0.0199	-0.0179	-0.0104	-0.0068	-0.0039
18227	-0.0211	-0.0216	-0.0149	-0.0071	-0.0047
18236	-0.0025	-0.0109	-0.0097	-0.0056	-0.0044
18237	-0.0166	-0.0206	-0.0148	-0.0082	-0.0039
Mean	-0.0150	-0.0177	-0.0125	-0.0069	-0.0042
8202	-0.0125	-0.0056	-0.0048	-0.0025	-0.0011
8204	0.0030	0.0012	0.0003	-0.0007	-0.0012
8205	-0.0031	-0.0110	-0.0044	-0.0016	-0.0006
Mean	-0.0042	-0.0051	-0.0030	-0.0016	-0.0010
Combined Mean	-0.0104	-0.0123	-0.0084		

¹Values derived from difference (run 2—run 1) in resistance ratio values given in table 3.

²Values expressed in terms of t' .

Table 8. Derived values of t' at AU, AG, and AL.^{1,2}

Run 1 coefficients; run 2 $W(AU)$, $W(AG)$, $W(AL)$			
RT no.	$t'(AU)$	$t'(AG)$	$t'(AL)$
80179	1062.5003	960.5184	660.3975
18227	1062.4917	960.5051	660.3925
18236	1062.5146	960.5286	660.4017
18237	1062.4581	960.4925	660.3898
8202	1062.4934	960.5120	660.4034
8204	1062.5262	960.5373	660.4158
8205	1062.4781	960.5032	660.4052
Mean	1062.4946	960.5139	660.4008
SD ³	0.0225	0.0155	0.0087
Range	0.0681	0.0448	0.0260
Run 2 coefficients; run 1 $W(AU)$, $W(AG)$, $W(AL)$			
RT no.	$t'(AU)$	$t'(AG)$	$t'(AL)$
80179	1062.5340	960.5494	660.4178
18227	1062.5148	960.5314	660.4155
18236	1062.5026	960.5313	660.4145
18237	1062.5094	960.5420	660.4203
8202	1062.5188	960.5280	660.4135
8204	1062.5068	960.5244	660.4130
8205	1062.4922	960.5230	660.4127
Mean	1062.5112	960.5328	660.4153
SD	0.0132	0.0096	0.0028
Range	0.0418	0.0264	0.0076

$${}^1W(t')=1+At'+Bt'^2.$$

²Values of t' derived from indicated values of $W(FP)$ in table 3 and indicated values of the coefficients in table 4.

³SD: estimate of standard deviation of one value in set.

Table 9. Statistics of t'' at silver point.^{1,2}

RT set		Run 1	Run 2	Combined runs
NIM	Mean	960.5269	960.5240	960.5254
	SD ³	0.0052	0.0042	0.0046
	Range	0.0121	0.0103	0.0139
NBS	Mean	960.5211	960.5200	960.5206
	SD	0.0063	0.0009	0.0041
	Range	0.0124	0.0018	0.0124
Com- bined set	Mean	960.5244	960.5223	960.5233
	SD	0.0060	0.0038	0.0049
	Range	0.0171	0.0103	0.0171

¹ $W(t'')=1+at''+bt''^2$, where the coefficients a and b are determined from values of $W(AL)$ and $W(AU)$ given in table 6, and $t''(AL)=660.408$, $t''(AU)=1062.503$ (see table 6).

²Values of $t''(AG)$ derived from values of $W(AG)$ given in table 3 using the above equation.

³SD: estimate of standard deviation of one value in indicated set.

the difference between the largest and the smallest of its six $R(TP)$ values in a run. The other two statistics, "Max" and "RMS," deal with successive differences between values of $R(TP)$ in a given run. These successive differences are of interest because the value of $W(FP)$ is calculated from the mean of successive values of $R(TP)$ bracketing a value of $R(FP)$. "Max" is the largest of such successive differences in a run, without regard to sign of the difference. "RMS" is the square root of the mean of the squares of such successive differences.

5.2 Second Experiment

The data obtained in the second experiment may be examined by plotting thermometer resistance as a func-

Table 10. Variations in $R(TP)$.¹
(Values given are parts in 10^6)²

RT no.	Run 1			Run 2		
	Range ³	Max ⁴	RMS ⁵	Range	Max	RMS
80179	5.6	4.8	3.2	7.6	5.0	3.0
18227	2.8	2.5	1.4	2.0	2.0	1.6
18236	4.8	4.8	2.9	2.6	1.7	1.1
18237	3.2	3.2	2.3	6.1	2.9	1.9
8202	8.3	5.5	2.9	2.5	2.5	1.9
8204	7.0	4.0	2.3	5.7	5.0	3.2
8205	3.8	2.3	1.4	9.5	5.5	3.1

¹Values derived from values of $R(TP)$ in tables A1a-g.

²A fractional difference in $R(TP)$ of 4×10^{-6} is equivalent to a temperature interval of about 1 mK at the triple point of water.

³Range: fractional difference between largest and smallest value of $R(TP)$ in a single run.

⁴Max: magnitude of largest fractional difference between two successive values of $R(TP)$ in a single run.

⁵RMS: root-mean-square of fractional differences between successive values of $R(TP)$ in a single run.

tion of time. Figures 3–8 are plots of the data given in tables A2a-f. The data points show results of the various electrical guard configurations; the data for each are connected by solid lines to form “freezing curves” of the silver as it solidified. For the NIM thermometers, the only possible guard configurations were with the external guard connected to or disconnected from the bridge

guard driving circuit, since the thermometers had no internal guarding system. The NBS thermometers were measured with both the internal and external guards connected to the drive circuit, with only the external guard connected, with only the internal guard connected, or with neither guard connected. The various configurations are labeled in the figures. The temperature scaling brackets shown in the figures are estimated from the relation

$$\Delta t = (\Delta R / R) \times W / (dW/dt), \quad (6)$$

where R is thermometer resistance at the silver point, W is $W(AG)$ taken from table 3, and the derivative dW/dt , found by differentiating eq (3), is evaluated at the silver point using the coefficients in table 4 and the mean value of $t'(AG)$ in table 6.

5.3 Third Experiment

The data obtained in the third experiment may also be examined by plotting. In this case the differences between thermometer indications at full immersion and at reduced immersion are plotted as a function of immersion. We start by computing for each thermometer the resistance differences,

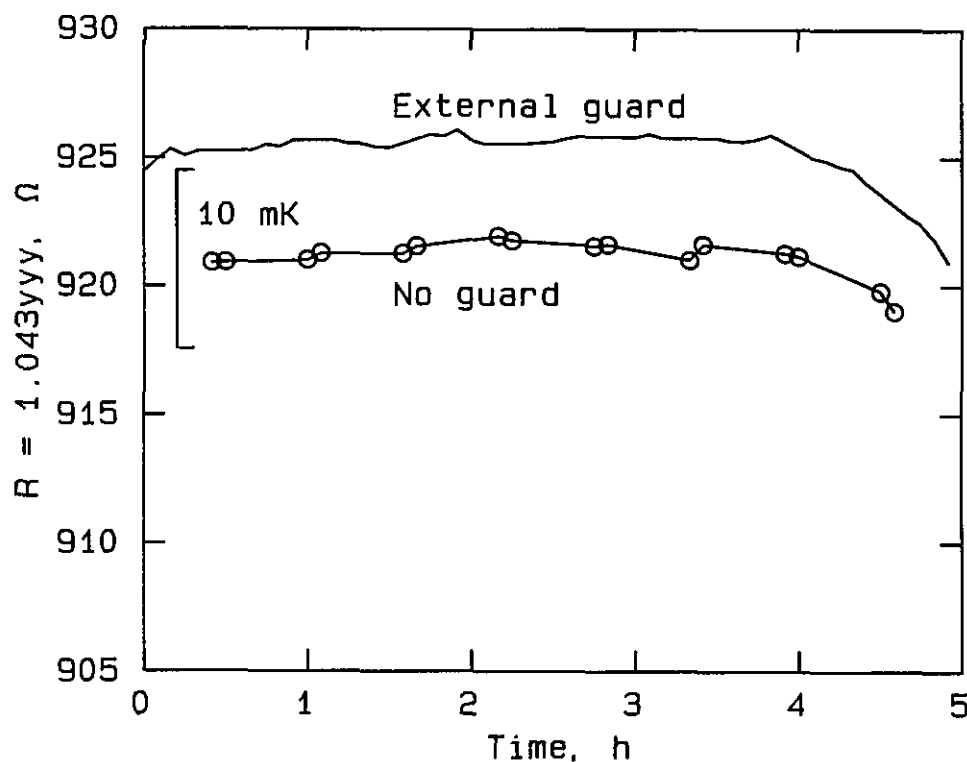


Figure 3—Effect of guarding at silver point, RT No. 80179, plotted from the data in table A2a. The curve labeled “External guard” represents measurements taken with the external guard connected to the bridge guard circuit. The curve labeled “No guard” represents measurements taken with the guard disconnected.

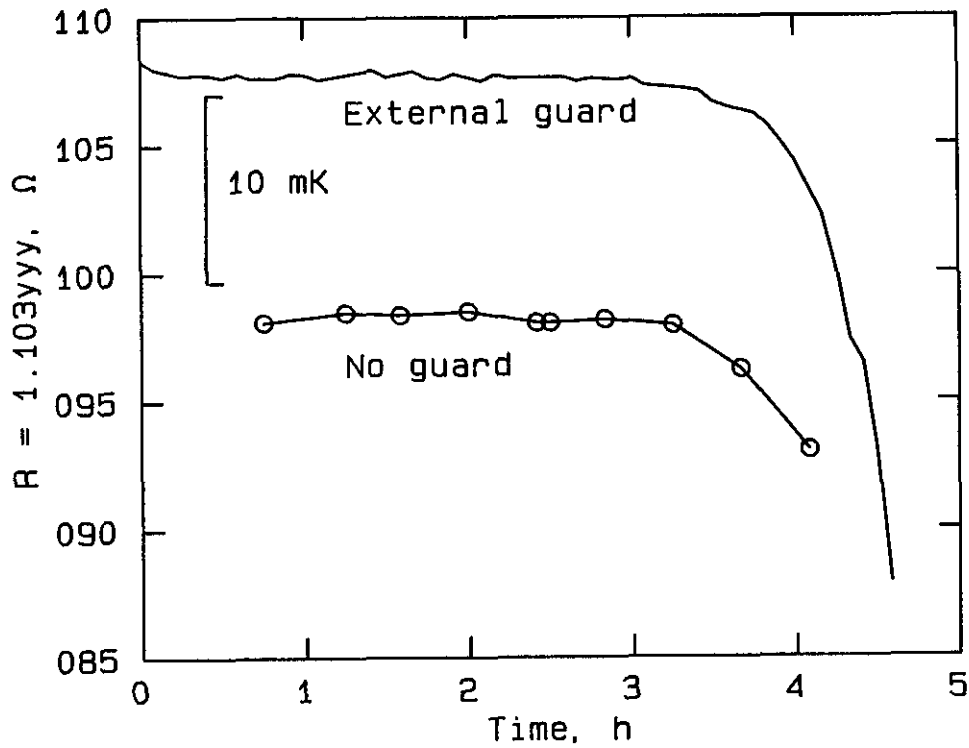


Figure 4—Effect of guarding at silver point, RT No. 18236, plotted from the data in table A2b. The curve labeled “External guard” represents measurements taken with the external guard connected to the bridge guard circuit. The curve labeled “No guard” represents measurements taken with the guard disconnected.

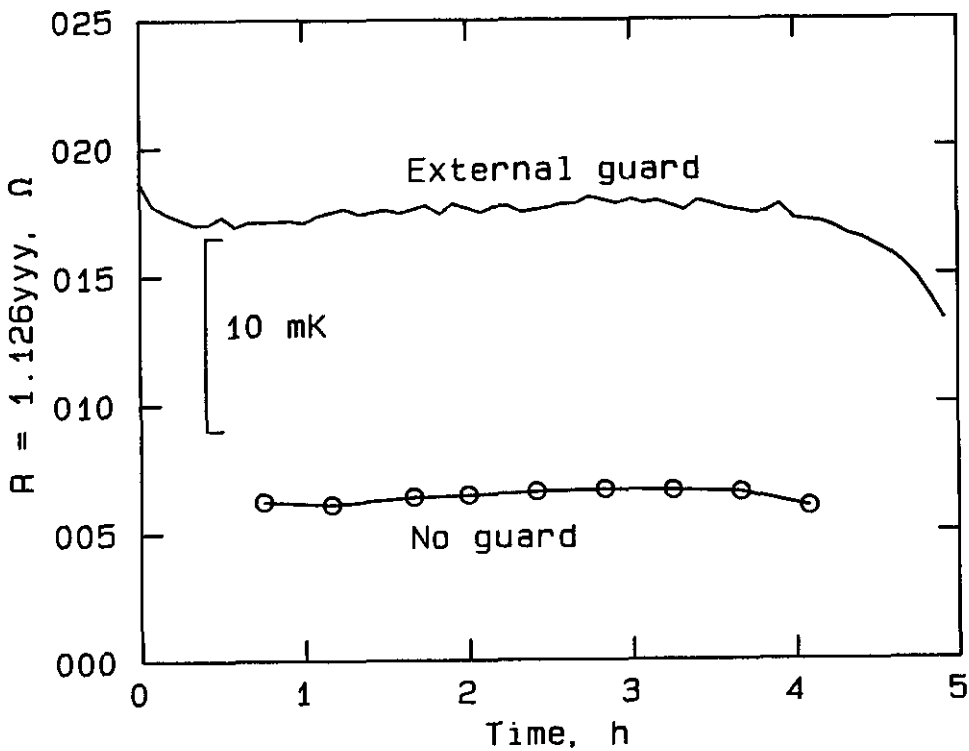


Figure 5—Effect of guarding at silver point, RT No. 18237, plotted from the data in table A2c. The curve labeled “External guard” represents measurements taken with the external guard connected to the bridge guard circuit. The curve labeled “No guard” represents measurements taken with the guard disconnected.

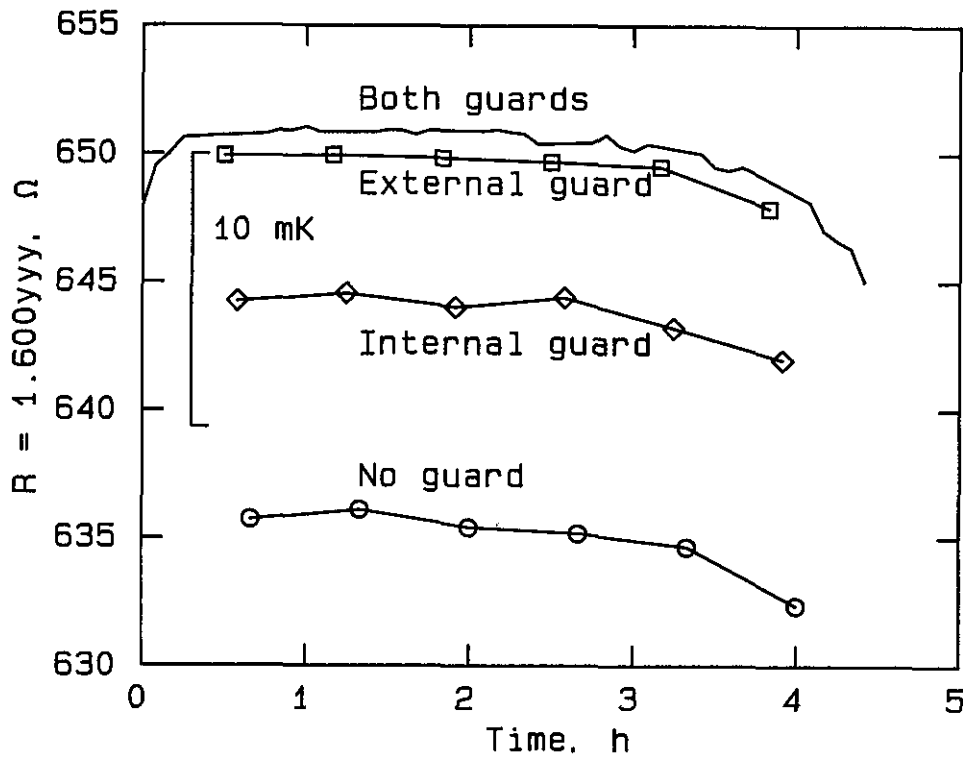


Figure 6—Effect of guarding at silver point, RT No. 8202, plotted from the data in table A2d. The curve labeled “Both guards” represents measurements taken with both the external guard and the internal thermometer guard connected to the bridge guard circuit. The curve labeled “External guard” represents measurements taken with only the external guard connected, and the curve labeled “Internal guard” represents measurements taken with only the internal guard connected. The curve labeled “No guard” represents measurements taken with neither guard connected to the bridge guard circuit.

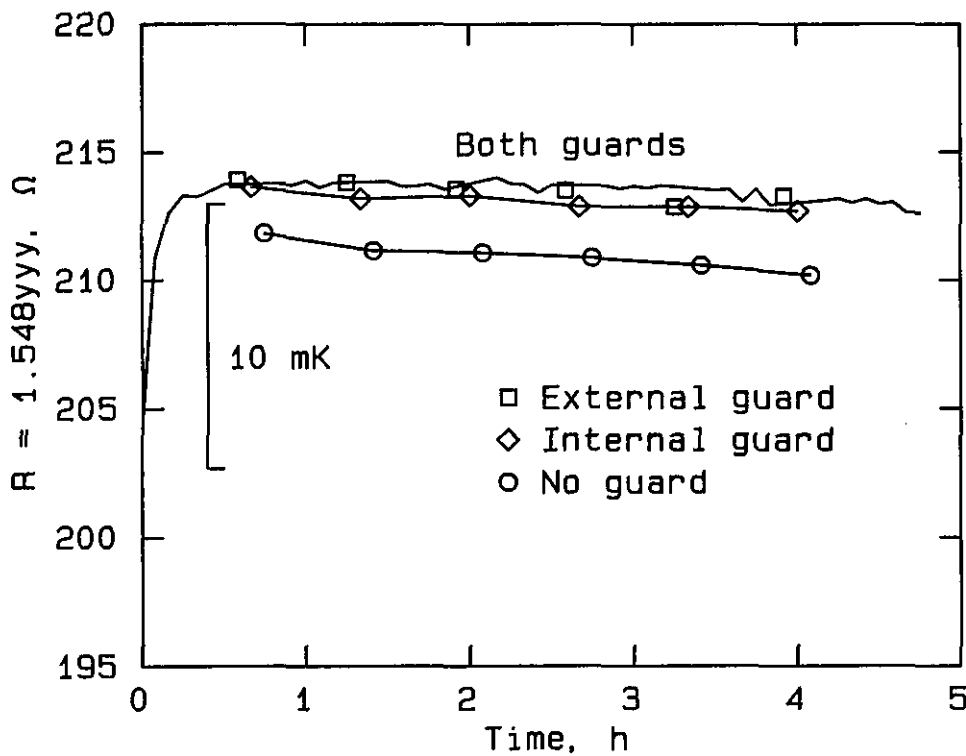


Figure 7—Effect of guarding at silver point, RT No. 8204, plotted from the data in table A2e. The curve labeled “Both guards” represents measurements taken with both the external guard and the internal thermometer guard connected to the bridge guard circuit. The unlabeled points lying on or close to the curve, designated by unconnected open symbols, represent measurements taken with only the external guard connected. The curve labeled “Internal guard” represents measurements taken with only the internal guard connected. The curve labeled “No guard” represents measurements taken with neither guard connected to the bridge guard circuit.

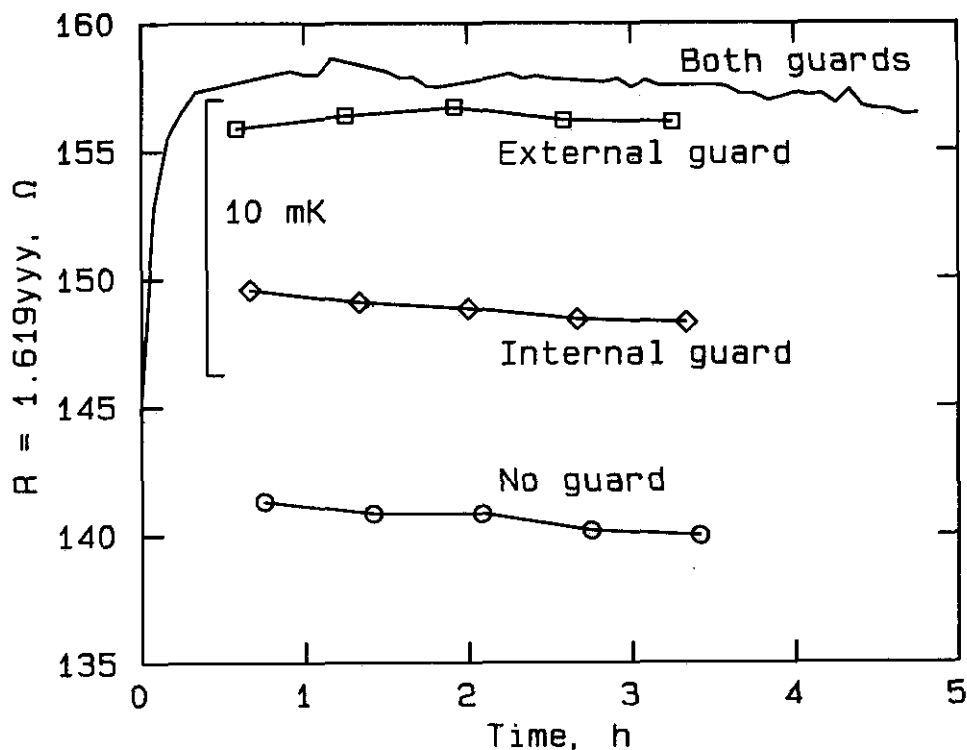


Figure 8—Effect of guarding at silver point, RT No. 8205, plotted from the data in table A2f. The curve labeled “Both guards” represents measurements taken with both the external guard and the internal thermometer guard connected to the bridge guard circuit. The curve labeled “External guard” represents measurements taken with only the external guard connected, and the curve labeled “Internal guard” represents measurements taken with only the internal guard connected. The curve labeled “No guard” represents measurements taken with neither guard connected to the bridge guard circuit.

$$\Delta R = R(\text{station } x) - R(\text{station } 0), \quad (7)$$

from the data in tables A3a and A3b. $R(\text{station } x)$ is the resistance measured when the thermometer is at one of the stations above station 0. $R(\text{station } 0)$ is the average of resistance measurements at station 0 before and after the measurement at station x . The resistance differences are then converted to equivalent temperature differences using eq (6), but with the second term evaluated for the zinc point. The resulting temperature differences are plotted as a function of immersion station up to station 10 in figures 9 and 10. The straight line with intercept at $\Delta t = 0$ in the plots represents the expected decrease in temperature with immersion due to the hydrostatic pressure of the liquid metal.

6. Evaluation of Thermometer Characteristics

6.1 Long-Time Stability at High Temperature

The effect of 100 h exposure at 1100 °C upon the thermometers may be judged from the results presented in tables 3–10. Changes in derived values can be ob-

served, and the group of thermometers as a whole tends to exhibit a downward drift in resistance ratio upon exposure (see tables 3 and 7). The results in table 7 show average changes for the group as a whole to be equivalent to 10.4 mK at the gold point, 12.3 mK at the silver point, and 8.4 mK at the aluminum point after the 100 h exposure. A comparison of the results in table 6 and 8, based on run 1 “calibration coefficients,” shows an increase in the variability of extrapolated values of t' after the exposure.

However, the thermometers are apparently not degraded in their ability to measure values on the designated “temperature scale” because of the exposure, as shown by a comparison of the statistics for run 1 and run 2 in table 6. Upon “recalibration” at the tin and zinc points, the mean extrapolated values of t' at the gold, silver, and aluminum points in run 2 differ little from the values obtained in run 1; the differences are 4.1, 5.7, and 2.3 mK respectively. Similarly, the statistics in table 9 show a change of only 2.1 mK in the mean value of t' at the silver point. As to thermometer variability, the statistics show the variability of t' , after recalibration, actually to be less in run 2 than in run 1. This is attributed more to a somewhat better precision in measurements in run 2 than to an effect of the exposure. Table 10 shows little difference in the variability of $R(\text{TP})$ due to exposure.

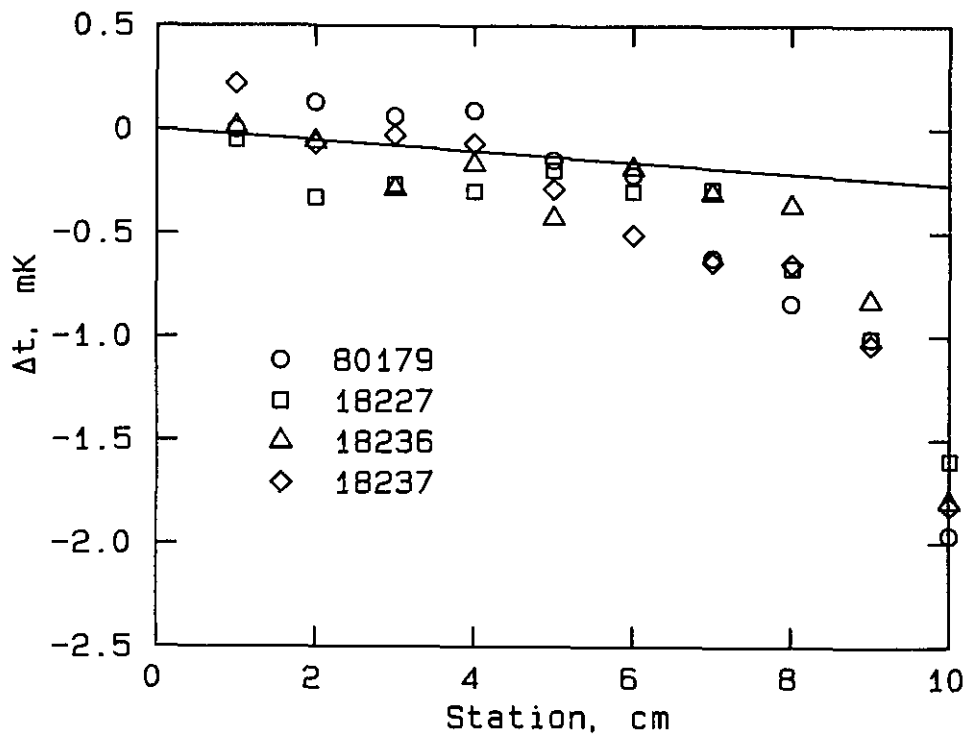


Figure 9—Effect of immersion in zinc cell at the freezing point, NIM thermometers, plotted from the data in table A3a. “Station” is the vertical location of the thermometer in the cell well; it represents the elevation of the thermometer, in cm, above full immersion. The thermometer is fully immersed and resting on the bottom of the cell well at station 0. Δt is the temperature equivalent of the difference in thermometer resistance, measured when the thermometer is fully immersed at station 0 and when it is elevated to the indicated station. The straight line represents the expected temperature gradient due to the hydrostatic pressure of the liquid zinc.

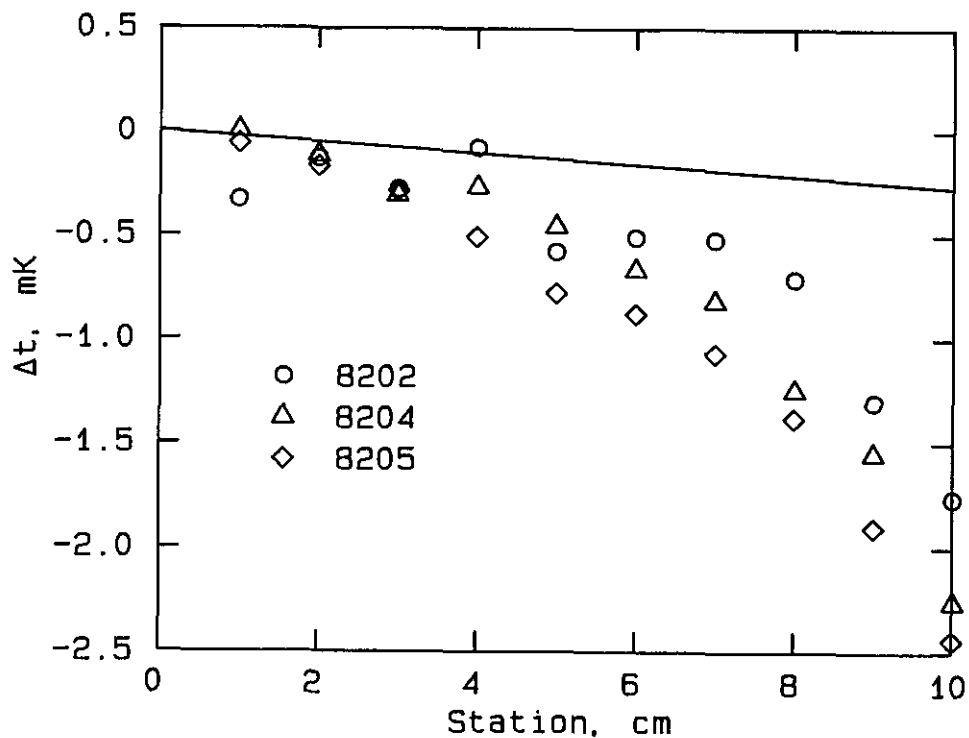


Figure 10—Effect of immersion in zinc cell at the freezing point, NBS thermometers, plotted from the data in table A3b. “Station” is the vertical location of the thermometer in the cell well; it represents the elevation of the thermometer, in cm, above full immersion. The thermometer is fully immersed and resting on the bottom of the cell well at station 0. Δt is the temperature equivalent of the difference in thermometer resistance, measured when the thermometer is fully immersed at station 0 and when it is elevated to the indicated station. The straight line represents the expected temperature gradient due to the hydrostatic pressure of the liquid zinc.

6.2 Short-Time Stability upon Temperature Cycling

The short-time stability of a thermometer subjected to the temperature cycling of either run in the first experiment, which is assumed to be typical for a thermometer calibration procedure, may be partially assessed from variations in the thermometer resistance at the triple point of water. The results are given in table 10. The variability of resistance ratios will depend in part on the variability of $R(TP)$, since a resistance ratio is derived from the mean of before and after $R(TP)$ determinations. Thus, the root-mean-square variations of $R(TP)$ given in the table could be expected to contribute the following temperature equivalents to the standard deviation of a determination of $W(FP)$: 0.9 to 2.7 mK at the gold point, 0.8 to 2.4 mK at the silver point, 0.6 to 1.7 mK at the aluminum point.

6.3 Temperature Coefficient of Resistance

The high values of the alpha coefficient given in table 4 show that the platinum in all of the thermometers is very pure and in a well defined physical state. The changes in alpha coefficients produced by the 100 h exposure at 1100 °C are consistent with the changes observed in resistance ratios at the fixed points.

6.4 Immersion Characteristics

The results of the third experiment provide some information about thermometer immersion characteristics. It must be emphasized that immersion behavior depends not only on thermometer characteristics, but also on details of the environment surrounding the thermometer. Figures 9 and 10 show the immersion behavior of the thermometers in the zinc cell.

The set of NIM thermometers appears to "track" the temperature gradient produced by hydrostatic pressure over the bottom 4 cm of immersion, while the set of NBS thermometers probably tracks the gradient over the bottom 2 cm of immersion. Consequently, immersion losses at the zinc point are probably not a major source of error in the temperature determinations with any of the thermometers. While it is believed that immersion losses at other fixed points used in the experiments are not a limiting source of error, a more thorough examination of thermometer immersion behavior in all of the fixed-point cells would be highly desirable, if measurements could be made with adequate precision (see below).

6.5 Heating Effect of Measuring Current

Heating effects at all fixed points are listed in tables A1a through A1g. It may be noted that the heating effect in the NIM thermometers due to the 4 mA measuring current is small and almost negligible. The larger heating effect in the NBS thermometers (and also the poorer immersion characteristic noted above) is attributable to resistor design; half the resistor wire is remote from the wall of the thermometer sheath in the toroidal resistor.

6.6 Electrical Leakage of Thermometer Supporting Parts

The results of the second experiment, plotted in figures 3 through 8, provide some information about the effects of electrical leakage in the thermometers. The experiment takes advantage of the electrical guard driving circuit available in the automatic bridge used. The internal guard system in the guarded lead thermometers (NBS) reduces the error due to electrical leakage from lead to lead in the thermometer, and from the thermometer leads to the bridge through ground. It does not, however, prevent leakage at the unguarded resistor. The external guard temporarily installed on the thermometers reduces only the effects due to leakage through ground between the thermometer and the grounded bridge.

It is evident from the data that leakage through ground is a major source of error in all of the thermometers when they are measured with a grounded instrument, and that the internal guard system used only partially eliminates the error. Without any guarding, leakage effects at the silver point can amount to 20 mK or more. In other preliminary tests with internally guarded thermometers, it has been found that the effect is even greater at the gold point, but may be very small at the aluminum point. The data do not reveal whether the external guard completely eliminates the leakage through ground.

The data show that the effect can vary considerably from thermometer to thermometer. The effect may also vary from time to time in a particular thermometer. It has been observed that in some thermometers, in the absence of an external guard, a small movement of the thermometer during measurement in a high temperature fixed-point cell can alter the electrical leakage. The effect thus adds to the imprecision of measurements, and, in experiments such as immersion tests in the cells, may obscure results.

6.7 Thermometer Durability

The thermometers experienced no catastrophic failures and no obvious *mechanical degradation* during the course of the experiments. The bending of support blades in two of the NIM thermometers and the separation of a lead in one of the NBS thermometers during initial stabilization suggest potential problem areas in the two designs.

6.8 Agreement Among Thermometers of Derived Temperature Values

The agreement among thermometers has been tested by means of two "temperature scales." For one scale, on which values of temperature are designated by the symbol t' , the thermometers are "calibrated" at the tin and zinc points, and then the values of temperature are determined at the aluminum, silver, and gold points by extrapolation. For the other scale, on which the thermometers are "calibrated" at the aluminum and gold points, the values of temperature (designated by the symbol t'') at the silver point are determined by interpolation. These procedures allow comparison of derived values at the available constant-temperature fixed points, and the measures of variability given in tables 6 and 9 describe the agreement among thermometers using the procedures.

It is unlikely that a practical temperature scale at high temperatures would be defined by extrapolation from lower temperatures, as in the case of the " t' scale." Such a procedure exaggerates the variability in derived temperature values due to propagation of normal and unavoidable calibration errors. It is more likely that a practical scale will be devised so that values of temperature can be derived by interpolation between adjacent defining fixed points, as in the case of the " t'' scale". Table 9 shows a smaller variability in t'' at the silver point (an interpolated value) than is shown in table 6 for t' at the silver point (an extrapolated value). A practical temperature scale utilizing all of the fixed points, including the silver point, could be expected to exhibit even less variability in derived temperature values. Therefore, the variations among thermometers reported here are larger than would be expected with the use of a well-designed temperature scale; the variations should be considered as upper bounds on thermometer variability.

Despite its limitations, the " t' scale" is useful for comparison purposes because of its simplicity and because the data necessary for deriving values on it are often available. In the present case, it reveals little difference between the two groups of thermometers, and in fact, all seven thermometers may be considered as a single set. It

is interesting to compare these results with results obtained earlier using other sets of thermometers. This is done in table 11, where the results obtained with 2.5-ohm guarded-lead thermometers measured with the grounded automatic bridge [3], and the results obtained with 0.25-ohm unguarded "birdcage" thermometers measured with isolated dc instrumentation [11], are summarized along with the present results. The summary shows differences between mean values at the fixed points that may be attributable, at least in part, to leakage problems. The summary also shows a decreasing variability in measurements in the past decade, though the decrease is not very dramatic.

Table 11. Statistics of t' at fixed points.

RT set		AU	AG	AL
NIM/NBS ¹ (14/7) 1984	Mean	1062.5030	960.5233	660.4080
	SD ⁴	0.0148	0.0097	0.0037
	Range	0.0485	0.0296	0.0149
NBS 2.5 ohm ² (11,16/8) 1982	Mean	1062.4898	960.5154	660.4127
	SD	0.0114	0.0079	0.0024
	Range	0.0341	0.0243	0.0088
Birdcage ³ (27/9) 1971	Mean	1062.5308	960.5230	— — — —
	SD	0.0191	0.0132	(0.0032)
	Range	0.0816	0.0541	(0.0087)

¹NIM/NBS: 14 independent determinations at each of the fixed points with 7 thermometers, this report.

²NBS 2.5 ohm: 11 independent determinations at AU, 16 independent determinations at AG and AL with 8 thermometers, reported [3] in 1982.

³Birdcage: 27 independent determinations at AU, AG, and the antimony point with 9 thermometers, reported [11] in 1971.

⁴SD: estimate of standard deviation of one value in indicated set.

7. Summary and Conclusions

The results of the experiments reported here show that the two sets of high-temperature platinum resistance thermometers tested, thermometers from different sources and of different design, behaved in a similar manner. The thermometers proved to be enough alike in their characteristics and performance that they could be considered as a single class.

It was found that upon prolonged exposure to high temperature the resistance ratios of the thermometers, on the average, changed by the equivalent of only 8 to 12 mK at high temperature fixed points. The exposure (100 h at 1100 °C) was probably more severe than that to which thermometers would normally be subjected.

The thermometers were subjected to cycling between high temperatures and room temperature, comparable to cycling that would be encountered in normal use and

calibration. The variability in thermometer resistance at the triple point of water with such cycling, expressed as a root-mean-square relative change in resistance per cycle, was found to range from about 1 to 3 parts in 10^6 . This variability in resistance is equivalent to temperature increments of 0.3 to 0.8 mK at the triple point; it would contribute the equivalent of about 1 to 3 mK to the variability of resistance ratios at the gold point derived from the mean of bracketing triple-point determinations.

The thermometers proved to be durable; the 100-h exposure produced no pronounced mechanical change in them, and throughout the tests their alpha coefficients remained greater than 0.0039268 K^{-1} . Self-heating effects and immersion characteristics of the thermometers were found to be commensurate with thermometer design and not to be accuracy-limiting sources of error. When the thermometers were calibrated on a simple quadratic "temperature scale" and values determined by extrapolation to high temperatures, the standard deviation of a single thermometer measurement was estimated to be about 4 mK at the aluminum point, 10 mK at the silver point, and 15 mK at the gold point. These values were found to compare favorably with values determined in the past by other sets of low resistance thermometers.

In contrast, it was found that electrical leakage through ground, between a thermometer at high temperature and a grounded measuring instrument, introduced large errors. Errors equivalent to 20 mK or more were observed at the silver point, and even greater errors were indicated at the gold point. Internal guarding of thermometer leads only partially eliminated the leakage, while the use of an electrical guard outside the thermometer appeared to be more effective. Consequently, the results reported here are probably biased by errors due to leakage effects, and variations in the leakage have also probably contributed to measurement imprecision. Electrical leakage through ground is believed to be the single largest source of error in the experiments.

Despite the problems with electrical leakage, it may be concluded from the results of the experiments that the thermometers tested are as good as or better than other thermometers tested in the past. A prior assessment has placed an uncertainty of about 10 mK on "state-of-the-art" resistance thermometer measurements up to the gold point [14]. In view of their exceptional long-time stability, agreement in derived temperature values, and other favorable characteristics, the present thermometers could be expected to perform equally as well, or better, if they were used so as to eliminate biases due to leakage.

References

- [1] Ling Shankang; Zhang Guoquan; Li Ruisheng; Wang Zilin; Li Zhiran; Zhao Qi; and Li Xumo. The development of temperature standards at NIM of China, chapter in *Temperature, its measurement and control in science and industry*, Vol. 5, part 1. J. F. Schooley, ed.-in-chief. New York: American Institute of Physics; 1982. 191–195.
- [2] Long Guang, and Tao Hongtu. Stability of precision high temperature platinum resistance thermometer, chapter in *Temperature, its measurement and control in science and industry*, Vol. 5, part 2. J. F. Schooley, ed.-in-chief. New York: American Institute of Physics; 1982. 783–787.
- [3] Evans, J. P. Experiences with high-temperature platinum resistance thermometers, chapter in *Temperature, its measurement and control in science and industry*, Vol. 5, part 2. J. F. Schooley, ed.-in-chief. New York: American Institute of Physics; 1982. 771–781.
- [4] Li Xumo; Zhang Jinde; Su Jinrong; and Chen Deming. A new high-temperature platinum resistance thermometer. *Metrologia* 18 (4): 203–208; 1982 December.
- [5] Bass, N. Construction of the NBS-design high-temperature platinum resistance thermometer, part 1 of *Techniques in high-temperature resistance thermometry*. Natl. Bur. Stand. (U.S.) Tech. Note 1183; 1984 January.
- [6] Evans, J. P., and Tillett, S. B. Toroidal resistor for high-temperature platinum resistance thermometers, part 2 of *Techniques in high-temperature resistance thermometry*. Natl. Bur. Stand. (U.S.) Tech. Note 1183; 1984 January.
- [7] Berry, R. J. The influence of crystal defects in platinum on platinum resistance thermometry, chapter in *Temperature, its measurement and control in science and industry*, Vol. 4, part 2. Harmon H. Plumb, ed.-in-chief; L. G. Rubin, ed. Pittsburgh: Instrument Society of America; 1972. 937–949.
- [8] Berry, R. J. Evaluation and control of platinum oxidation errors in standard platinum resistance thermometers, chapter in *Temperature, its measurement and control in science and industry*, Vol. 5, part 2. J. F. Schooley, ed.-in-chief. New York: American Institute of Physics; 1982. 743–752.
- [9] Evans, J. P., and D. M. Sweger. Immersion cooler for freezing ice mantles on triple-point-of-water cells. *Rev. Sci. Instr.* 40 (2): 376–377; 1969 February.
- [10] Furukawa, G. T. Investigation of freezing temperature of National Bureau of Standards aluminum standards. *J. Res. Natl. Bur. Stand. (U.S.)* 78A (4): 477–495; 1974 July–August.
- [11] Evans, J. P., and S. D. Wood. An intercomparison of high temperature platinum resistance thermometers and standard thermocouples. *Metrologia* 7 (3): 108–130; 1971 July.
- [12] Cutkosky, R. D. An automatic resistance thermometer bridge. *IEEE Trans. Instrum. Meas.* IM-13 (4): 330–333; 1980 December.
- [13] Cutkosky, R. D. Guarding techniques for resistance thermometers. *IEEE Trans. Instrum. Meas.* IM-30 (3): 217–220; 1981 September.
- [14] Evans, J. P. High temperature platinum resistance thermometry, chapter in *Temperature, its measurement and control in science and industry*, Vol. 4, part 2. Harmon H. Plumb, ed.-in-chief; L. G. Rubin, ed. Pittsburgh: Instrument Society of America; 1972. 899–906.

APPENDIX

Table A1a. Resistance of thermometer 80179 at fixed points.

FP ¹	Run 1			Run 2		
	$R(TP)^2$	$R(FP)^3$	HE(4) ⁴	$R(TP)$	$R(FP)$	HE(4)
TP	0.24354530		10	0.24355153		23
AU		1.11338142	17		1.11339495	30
TP	0.24354484		37	0.24355032		19
AG		1.04390980	22		1.04391980	11
TP	0.24354602		10	0.24355100		4
AL		0.82218768	15		0.82219719	20
TP	0.24354487		19	0.24355033		1
ZN		0.62563109	15		0.62563938	9
TP	0.24354467		22	0.24355013		8
SN		0.46097202	24		0.46097844	28
TP	0.24354465		16	0.24354968		14

¹Measurements taken in order indicated.

² $R(TP)$: thermometer resistance (ohms) at triple point of water for zero measuring current.

³ $R(FP)$: thermometer resistance (ohms) at indicated metal freezing point for zero measuring current.

⁴HE(4): increase in resistance of thermometer (ohms $\times 10^{-8}$) due to heating effect of 4 mA measuring current.

Table A1b. Resistance of thermometer 18227 at fixed points.

FP ¹	Run 1			Run 2		
	$R(TP)^2$	$R(FP)^3$	HE(4) ⁴	$R(TP)$	$R(FP)$	HE(4)
TP	0.26036578		17	0.26036839		23
AU		1.19023546	41		1.19023032	24
TP	0.26036617		8	0.26036787		29
AG		1.11596340	14		1.11595591	6
TP	0.26036605		15	0.26036834		4
AL		0.87894006	14		0.87893466	19
TP	0.26036600		27	0.26036791		11
ZN		0.66881872	38		0.66881738	6
TP	0.26036586		10	0.26036793		16
SN		0.49279685	26		0.49279604	24
TP	0.26036652		19	0.26036836		5

^{1,2,3,4}See footnotes of Table A1a.

Table A1c. Resistance of thermometer 18236 at fixed points.

FP ¹	Run 1			Run 2		
	$R(TP)^2$	$R(FP)^3$	HE(4) ⁴	$R(TP)$	$R(FP)$	HE(4)
TP	0.25736827		1	0.25737145		17
AU		1.17651167	38		1.17652127	27
TP	0.25736951		17	0.25737131		16
AG		1.10310634	20		1.10310718	14
TP	0.25736898		21	0.25737129		18
AL		0.86881563	23		0.86881446	42
TP	0.25736916		10	0.25737091		17
ZN		0.66111513	26		0.66111592	14
TP	0.25736839		18	0.25737114		13
SN		0.48712186	19		0.48712267	24
TP	0.25736902		4	0.25737158		11

^{1,2,3,4}See footnotes of Table A1a.

Table A1d. Resistance of thermometer 18237 at fixed points.

FP ¹	Run 1			Run 2		
	<i>R</i> (TP) ²	<i>R</i> (FP) ³	HE(4) ⁴	<i>R</i> (TP)	<i>R</i> (FP)	HE(4)
TP	0.26271185		20	0.26271457		0
AU		1.20094154	45		1.20093838	42
TP	0.26271268		5	0.26271380		7
AG		1.12601457	23		1.12600557	14
TP	0.26271186		16	0.26271372		2
AL		0.88685765	35		0.88685013	14
TP	0.26271188		14	0.26271298		18
ZN		0.67484408	23		0.67483947	20
TP	0.26271194		9	0.26271309		19
SN		0.49723614	30		0.49723423	20
TP	0.26271258		4	0.26271339		10

^{1,2,3,4}See footnotes of Table A1a.

Table A1e. Resistance of thermometer 8202 at fixed points.

FP ¹	Run 1			Run 2		
	<i>R</i> (TP) ²	<i>R</i> (FP) ³	HE(4) ⁴	<i>R</i> (TP)	<i>R</i> (FP)	HE(4)
TP	0.37344847		82	0.37345575		77
AU		1.70715643	123		1.70717762	121
TP	0.37344900		72	0.37345655		87
AG		1.60063481	87		1.60065483	89
TP	0.37345106		67	0.37345562		102
AL		1.26069404	98		1.26070485	100
TP	0.37345126		70	0.37345654		92
ZN		0.95931356	117		0.95932446	84
TP	0.37345063		84	0.37345639		84
SN		0.70683891	120		0.70684723	92
TP	0.37345157		69	0.37345619		86

^{1,2,3,4}See footnotes of Table A1a.

Table A1f. Resistance of thermometer 8204 at fixed points.

FP ¹	Run 1			Run 2		
	<i>R</i> (TP) ²	<i>R</i> (FP) ³	HE(4) ⁴	<i>R</i> (TP)	<i>R</i> (FP)	HE(4)
TP	0.36121077		58	0.36121424		50
AU		1.65121770	97		1.65124068	86
TP	0.36121028		72	0.36121557		56
AG		1.54818827	90		1.54820525	64
TP	0.36121172		55	0.36121378		65
AL		1.21938181	82		1.21938917	91
TP	0.36121142		66	0.36121351		64
ZN		0.92787383	94		0.92787912	104
TP	0.36121198		74	0.36121466		72
SN		0.68367531	88		0.68367855	102
TP	0.36121282		59	0.36121529		62

^{1,2,3,4}See footnotes of Table A1a.

Table A1g. Resistance of thermometer 8205 at fixed points.

FP ¹	Run 1			Run 2		
	R(TP) ²	R(FP) ³	HE(4) ⁴	R(TP)	R(FP)	HE(4)
TP	0.37777464		77	0.37777391		94
AU		1.72688249	105		1.72688057	103
TP	0.37777472		80	0.37777600		77
AG		1.61914245	88		1.61913827	89
TP	0.37777384		87	0.37777615		85
AL		1.27526979	106		1.27527344	97
TP	0.37777447		89	0.37777749		62
ZN		0.97040708	124		0.97041140	102
TP	0.37777487		85	0.37777686		84
SN		0.71501507	117		0.71501814	111
TP	0.37777526		75	0.37777734		80

^{1,2,3,4}See footnote of Table A1a.

Table A2a. Effect of guarding at silver point, thermometer 80179.

No. ¹	Thermometer resistance ²		No.	Thermometer resistance	
	External Guard	No Guard		External Guard	No Guard
1	1.04392444		31	1.04392563	
2	1.04392494		32	1.04392576	
3	1.04392533		33	1.04392585	
4	1.04392506		34		1.04392155
5	1.04392526		35		1.04392162
6		1.04392090	36	1.04392582	
7		1.04392092	37	1.04392580	
8	1.04392524		38	1.04392595	
9	1.04392531		39	1.04392578	
10	1.04392552		40	1.04392577	
11	1.04392542		41		1.04392101
12	1.04392569		42		1.04392163
13		1.04392100	43	1.04392580	
14		1.04392127	44	1.04392567	
15	1.04392567		45	1.04392564	
16	1.04392553		46	1.04392575	
17	1.04392556		47	1.04392592	
18	1.04392541		48		1.04392127
19	1.04392538		49		1.04392115
20		1.04392126	50	1.04392502	
21		1.04392155	51	1.04392489	
22	1.04392592		52	1.04392467	
23	1.04392583		53	1.04392454	
24	1.04392610		54	1.04392402	
25	1.04392569		55		1.04391980
26	1.04392554		56		1.04391904
27		1.04392194	57	1.04392274	
28		1.04392176	58	1.04392240	
29	1.04392554		59	1.04392180	
30	1.04392560		60	1.04392091	

¹ No.: sequence number of reading. Resistance determinations made at 5 min intervals.

² All determinations made with normal measuring current.

Table A2b. Effect of guarding at silver point, thermometer 18236.

No. ¹	Thermometer resistance ²		No.	Thermometer resistance	
	External Guard	No Guard		External Guard	No Guard
1	1.10310830		36	1.10310753	
2	1.10310798		37	1.10310762	
3	1.10310787		38	1.10310730	
4	1.10310773		39	1.10310727	
5	1.10310780		40		1.10309795
6	1.10310777		41	1.10310717	
7	1.10310766		42	1.10310708	
8	1.10310783		43	1.10310663	
9	1.10310764		44	1.10310644	
10		1.10309809	45		1.10309621
11	1.10310763		46	1.10310619	
12	1.10310782		47	1.10310571	
13	1.10310777		48	1.10310504	
14	1.10310757		49	1.10310429	
15	1.10310767		50		1.10309304
16		1.10309847	51	1.10310223	
17	1.10310786		52	1.10310018	
18	1.10310796		53	1.10309737	
19	1.10310766		54	1.10309643	
20		1.10309836	55	1.10309299	
21	1.10310790		56	1.10308788	
22	1.10310762		57	1.10307519	
23	1.10310756		58	1.10300411	
24	1.10310779		59	1.10234670	
25		1.10309850	60	1.10218298	
26	1.10310748		61	1.10208952	
27	1.10310777		62	1.10228282	
28	1.10310760		63	1.10229746	
29	1.10310764		64	1.10229948	
30		1.10309806	65	1.10228864	
31		1.10309806	66	1.10227829	
32	1.10310766		67	1.10225154	
33	1.10310748		68	1.10226344	
34	1.10310761		69	1.10225939	
35		1.10309818	70	1.10224858	

^{1,2} See footnotes of Table A2a.

Table A2c. Effect of guarding at silver point, thermometer 18237.

No. ¹	Thermometer resistance ²		No.	Thermometer resistance	
	External Guard	No Guard		External Guard	No Guard
1	1.12601866		13	1.12601706	
2	1.12601772		14	1.12601735	
3	1.12601741		15		1.12600610
4	1.12601719		16	1.12601762	
5	1.12601699		17	1.12601739	
6	1.12601702		18	1.12601746	
7	1.12601732		19	1.12601757	
8	1.12601692		20	1.12601742	
9	1.12601711		21		1.12600639
10		1.12600623	22	1.12601775	
11	1.12601713		23	1.12601739	
12	1.12601717		24	1.12601781	

Table A2c. Effect of guarding at silver point, thermometer 18237.—Continued

No. ¹	Thermometer resistance ²		No.	Thermometer resistance	
	External Guard	No Guard		External Guard	No Guard
25		1.12600647	49	1.12601716	
26	1.12601744		50		1.12600598
27	1.12601768		51	1.12601704	
28	1.12601773		52	1.12601684	
29	1.12601745		53	1.12601655	
30		1.12600659	54	1.12601641	
31	1.12601764		55	1.12601612	
32	1.12601779		56	1.12601584	
33	1.12601781		57	1.12601543	
34	1.12601807		58	1.12601487	
35		1.12600667	59	1.12601409	
36	1.12601779		60	1.12601322	
37	1.12601796		61	1.12601211	
38	1.12601778		62	1.12601112	
39	1.12601790		63	1.12601050	
40		1.12600662	64	1.12600944	
41	1.12601752		65	1.12600784	
42	1.12601792		66	1.12600536	
43	1.12601777		67	1.12600135	
44	1.12601760		68	1.12599782	
45		1.12600655	69	1.12599122	
46	1.12601740		70	1.12597467	
47	1.12601745		71	1.12561508	
48	1.12601774		72	1.12534593	

^{1,2} See footnotes of Table A2a.

Table A2d. Effect of guarding at silver point, thermometer 8202.

No. ¹	Thermometer resistance ²				No.	Thermometer resistance			
	Both Guards	External Guard	Internal Guard	No Guard		Both Guards	External Guard	Internal Guard	No Guard
1	1.60064788				25				1.60063539
2	1.60064955				26	1.60065087			
3	1.60065002				27	1.60065094			
4	1.60065063				28	1.60065082			
5	1.60065065				29	1.60065076			
6	1.60065069				30	1.60065037			
7		1.60064992			31		1.60064967		
8			1.60064424		32			1.60064438	
9				1.60063572	33				1.60063516
10	1.60065077				34	1.60065044			
11	1.60065091				35	1.60065075			
12	1.60065091				36	1.60065028			
13	1.60065105				37	1.60065012			
14	1.60065082				38	1.60065039			
15		1.60064994			39		1.60064949		
16			1.60064455		40			1.60064320	
17				1.60063609	41				1.60063464
18	1.60065083				42	1.60065000			
19	1.60065093				43	1.60064946			
20	1.60065089				44	1.60064935			
21	1.60065073				45	1.60064951			
22	1.60065092				46	1.60064924			
23		1.60064983			47		1.60064788		
24			1.60064400		48			1.60064197	

Table A2d. Effect of guarding at silver point, thermometer 8202.—Continued

No. ¹	Thermometer resistance ²				No.	Thermometer resistance			
	Both Guards	External Guard	Internal Guard	No Guard		Both Guards	External Guard	Internal Guard	No Guard
49				1.60063237	52	1.60064660			
50	1.60064810				53	1.60064631			
51	1.60064700				54	1.60064501			

^{1,2} See footnote of Table A2a.

Table A2e. Effect of guarding at silver point, thermometer 8204.

No. ¹	Thermometer resistance ²				No.	Thermometer resistance			
	Both Guards	External Guard	Internal Guard	No Guard		Both Guards	External Guard	Internal Guard	No Guard
1	1.54820421				30	1.54821341			
2	1.54821086				31	1.54821373			
3	1.54821266				32		1.54821351		
4	1.54821332				33			1.54821288	
5	1.54821325				34				1.54821089
6	1.54821350				35	1.54821369			
7	1.54821376				36	1.54821357			
8		1.54821392			37	1.54821368			
9			1.54821365		38	1.54821359			
10				1.54821185	39	1.54821371			
11	1.54821378				40		1.54821286		
12	1.54821371				41			1.54821287	
13	1.54821390				42				1.54821059
14	1.54821361				43	1.54821350			
15	1.54821382				44	1.54821356			
16		1.54821381			45	1.54821305			
17			1.54821318		46	1.54821356			
18				1.54821116	47	1.54821293			
19	1.54821386				48		1.54821328		
20	1.54821364				49			1.54821270	
21	1.54821367				50				1.54821020
22	1.54821375				51	1.54821312			
23	1.54821354				52	1.54821318			
24		1.54821355			53	1.54821301			
25			1.54821331		54	1.54821318			
26				1.54821108	55	1.54821297			
27	1.54821401				56	1.54821306			
28	1.54821376				57	1.54821263			
29	1.54821373				58	1.54821261			

^{1,2} See footnotes of Table A2a.

Table A2f. Effect of guarding at silver point, thermometer 8205.

No. ¹	Thermometer resistance ²				No.	Thermometer resistance			
	Both Guards	External Guard	Internal Guard	No Guard		Both Guards	External Guard	Internal Guard	No Guard
1	1.61914472				9			1.61914954	
2	1.61915280				10				1.61914129
3	1.61915553				11	1.61915803			
4	1.61915653				12	1.61915813			
5	1.61915731				13	1.61915796			
6	1.61915743				14	1.61915798			
7	1.61915755				15	1.61915860			
8		1.61915587			16		1.61915636		

Table A2f. Effect of guarding at silver point, thermometer 8205.—Continued

No. ¹	Thermometer resistance ²				No.	Thermometer resistance			
	Both Guards	External Guard	Internal Guard	No Guard		Both Guards	External Guard	Internal Guard	No Guard
17			1.61914904		38	1.61915773			
18				1.61914080	39	1.61915751			
19	1.61915808				40		1.61915609		
20	1.61915782				41			1.61914825	
21	1.61915787				42				1.61913994
22	1.61915749				43	1.61915756			
23	1.61915748				44	1.61915748			
24		1.61915669			45	1.61915719			
25			1.61914880		46	1.61915722			
26				1.61914080	47	1.61915693			
27	1.61915787				48	1.61915708			
28	1.61915801				49	1.61915726			
29	1.61915779				50	1.61915712			
30	1.61915791				51	1.61915721			
31	1.61915779				52	1.61915681			
32		1.61915617			53	1.61915736			
33			1.61914839		54	1.61915669			
34				1.61914015	55	1.61915660			
35	1.61915767				56	1.61915658			
36	1.61915781				57	1.61915638			
37	1.61915745				58	1.61915644			

^{1,2} See footnotes of Table A2a.

Table A3a. Immersion characteristics of thermometers in zinc cell.^{1,3}

Station ²		Resistance of thermometer number				Station		Resistance of thermometer number			
cm	80179	18227	18236	18237	cm	80179	18227	18236	18237		
	0	0.62564094	0.66881727	0.66111506	0.67483970	7	0.62563817	0.66881563	0.66111550	0.67483869	
	0	0.62564009	0.66881635	0.66111560	0.67483926	6	0.62563851	0.66881562	0.66111561	0.67483881	
	0	0.62563969	0.66881612	0.66111562	0.67483920	0	0.62563869	0.66881598	0.66111585	0.67483930	
	0	0.62563923	0.66881629	0.66111546	0.67483921	0	0.62563858	0.66881588	0.66111580	0.67483918	
18	0.62469878	0.66772854	0.65999691	0.67377628	0	0.62563850	0.66881599	0.66111593	0.67483931		
18	0.62468420	0.66769737	0.65997147	0.67371738	5	0.62563830	0.66881572	0.66111552	0.67483899		
16	0.62532066	0.66845569	0.66074723	0.67446863	4	0.62563851	0.66881563	0.66111576	0.67483919		
14	0.62555932	0.66871951	0.66101985	0.67474217	3	0.62563848	0.66881566	0.66111565	0.67483923		
12	0.62562814	0.66880302	0.66110364	0.67482532	2	0.62563854	0.66881561	0.66111586	0.67483919		
10	0.62563737	0.66881433	0.66111437	0.67483735	1	0.62563843	0.66881586	0.66111592	0.67483946		
0	0.62563886	0.66881583	0.66111589	0.67483939	0	0.62563836	0.66881582	0.66111589	0.67483920		
0	0.62563878	0.66881593	0.66111572	0.67483913	0	0.62563841	0.66881591	0.66111581	0.67483919		
0	0.62563872	0.66881580	0.66111571	0.67483926	0	0.62563846	0.66881569	0.66111578	0.67483930		
10	0.62563703	0.66881444	0.66111416	0.67483761	0	0.62563843	0.66881570	0.66111577	0.67483935		
9	0.62563784	0.66881497	0.66111503	0.67483833	0	0.62563840	0.66881587	0.66111591	0.67483913		
8	0.62563799	0.66881528	0.66111545	0.67483868							

¹Resistance determinations made at 5 min intervals.

²Station: distance (cm) thermometer raised above full immersion.

³All determinations made with normal measuring current.

Table A3b. Immersion characteristics of thermometers in zinc cell.^{1,3}

Station ²	Resistance of thermometer number		
	8202	8204	8205
0	0.95931822	0.92788595	0.97041322
0	0.95931846	0.92788611	0.97041326
0	0.95931850	0.92788615	0.97041342
0	0.95931844	0.92788625	0.97041309
18	0.95818532	0.92679249	0.96920870
18	0.95816807	0.92676693	0.96918238
16	0.95884974	0.92745293	0.96990494
14	0.95922028	0.92779867	0.97029903
12	0.95930572	0.92787549	0.97039663
10	0.95931639	0.92788322	0.97040958
0	0.95931885	0.92788618	0.97041311
0	0.95931879	0.92788625	0.97041361
0	0.95931866	0.92788612	0.97041344
0	0.95931875	0.92788634	0.97041330
10	0.95931649	0.92788339	0.97041009
9	0.95931708	0.92788429	0.97041080
8	0.95931786	0.92788468	0.97041149
7	0.95931810	0.92788521	0.97041190
6	0.95931812	0.92788541	0.97041214
0	0.95931881	0.92788616	0.97041331
0	0.95931876	0.92788638	0.97041326
0	0.95931920	0.92788636	0.97041333
0	0.95931870	0.92788626	0.97041335
5	0.95931818	0.92788564	0.97041231
4	0.95931882	0.92788588	0.97041266
3	0.95931856	0.92788584	0.97041295
2	0.95931876	0.92788607	0.97041311
1	0.95931850	0.92788622	0.97041325
0	0.95931916	0.92788619	0.97041332
0	0.95931833	0.92788620	0.97041322
0	0.95931903	0.92788607	0.97041312
0	0.95931882	0.92788632	0.97041306
0	0.95931895	0.92788615	0.97041351

^{1,2,3}See footnotes of Table A.3a.

Automated High-Temperature PVT Apparatus With Data for Propane

G. C. Straty

National Bureau of Standards, Boulder, CO 80303

and

A. M. F. Palavra

Instituto Superior Tecnico, Lisboa-1, Portugal

Accepted: June 20, 1984

An apparatus is described which can be used for PVT and compressibility measurements on supercritical fluids from near room temperature to 600 °C and pressures to 35 MPa. Two separate experimental techniques are employed to obtain PVT data over a broad range of the state surface. Burnett expansions are performed to generate compressibility factor (or equivalently density) data along a well-behaved supercritical isotherm. A series of isochoric measurements is then made to extend the temperature range. Densities assigned to the isochores are determined from their intersection with the previously measured Burnett isotherm or gravimetrically. A computer is used for experimental control and for data logging. Isochoric measurements lasting several days can be performed routinely and without operator attention. The apparatus has been tested on propane to a temperature of 325 °C. The density data, estimated accurate to ± 0.1 percent, are in excellent agreement with other existing data.

Key words: Burnett method; compressibility; density; fluids; propane; PVT behavior.

Introduction

Perhaps the single most important property of any compressible fluid is its PVT behavior. An accurate and precise description of the PVT surface can, in principle, be used to calculate most equilibrium properties. PVT data are also required to analyze experimental data on other quantities and to perform engineering design calculations on fluid handling systems. Wide range PVT data for the many technically important fluids at

elevated temperatures are, however, often scarce and in some cases are nonexistent.

We describe here an experimental apparatus that can be used for PVT determinations on fluids above room temperature. Two separate experimental techniques are used to obtain data over a broad range of the state surface (see fig. 1). The well known Burnett [1]¹ method of successive gas expansions is used to establish the density behavior for the fluid along a well-behaved supercritical isotherm. The maximum temperature of such measurements is, however, limited by such things as the compatibility of valve packings and the pressure transducer with the elevated temperatures. The measurement of pressure versus temperature along a nearly isochoric path (pseudo-isochores) in a second experiment is then used to extend the temperature range. Densities assigned to the pseudo-isochores can be determined from their intersection with the previously measured isotherms.

About the Authors, Paper: G. C. Straty is with the Chemical Engineering Science Division of the NBS National Engineering Laboratory, while A. M. F. Palavra serves with the Centro de Quimica Estrutural, Complexo Interdisciplinar, in Portugal's Instituto Superior Tecnico. The work they report on was carried out for the Department of Energy, Office of Basic Energy Sciences.

¹Figures in brackets indicate literature references and explanatory notes at the end of this paper.

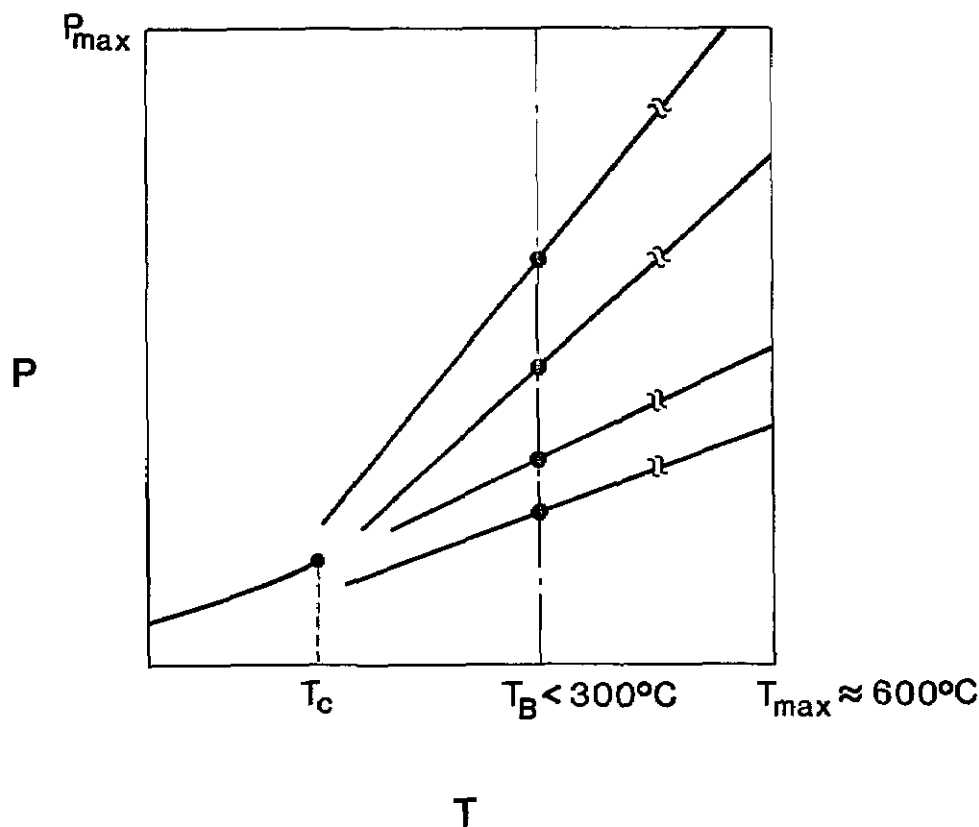


Figure 1.—Schematic of the P - T plane for a typical fluid. Densities along the T_B isotherm are obtained using a Burnett expansion technique. P - T measurements along pseudo isochores are then made to extend the temperature range from near critical temperature to T_{max} . Isochore densities are obtained from their intersection with the T_B isotherm.

Principal objectives in the design of the apparatus were: 1) the apparatus should be capable of measurements covering a broad temperature and pressure range, 2) the determined densities should be independent of the data accuracy for any calibration fluid, and 3) the apparatus should be automated as much as possible to minimize the necessity for operator attention.

The apparatus is capable of operation from near room temperature to about 600 °C at pressures to over 35 MPa. Densities can be determined by using two completely independent techniques, the Burnett method involving successive fluid expansions, or a gravimetric technique involving only the well known density of water used for volume calibration purposes. A small desktop computer is employed for experimental control, data logging, and partial real time data analysis. Measurement runs along isochores taking days to complete can be performed automatically and without operator attention.

Experimental

The experimental apparatuses are illustrated schematically in figure 2. The Burnett system [shown in a) and b) of fig. 2] consists of three spherical cells of different volumes and a diaphragm type differential pressure transducer with valving as shown. The cells with nomi-

nal volumes of about 200, 120 and 40 cm³ allow different volume ratios to be selected. These elements are suspended from a thermally insulated platen which forms the top closure to a thermostated bath used for temperature control. This arrangement is similar to that described previously in detail [2].

Mixed liquid baths are usually preferred and have traditionally been used for thermostating in this type of experiment. Because of the elevated temperatures of this work, however, a commercially available oven with vigorous circulation was modified for the purpose. Air is normally used as the convective heat transfer fluid but, for safety reasons, a continuous gas purge (typically nitrogen) is employed for work on flammable samples.

Even though the heat transfer gas is vigorously mixed, substantial temperature differences can exist over the oven volume. To minimize these differences, the components are encased in a massive aluminum block [not shown in a) of fig. 2 for clarity]. The typical arrangement is shown in b) of figure 2. Space is provided around each component to partially decouple it thermally from the block and to permit free flow of the heat transfer gas around the components. This arrangement reduces temperature differences to a few tenths of a degree. Further reduction in temperature differences is accomplished by using very low power shimming

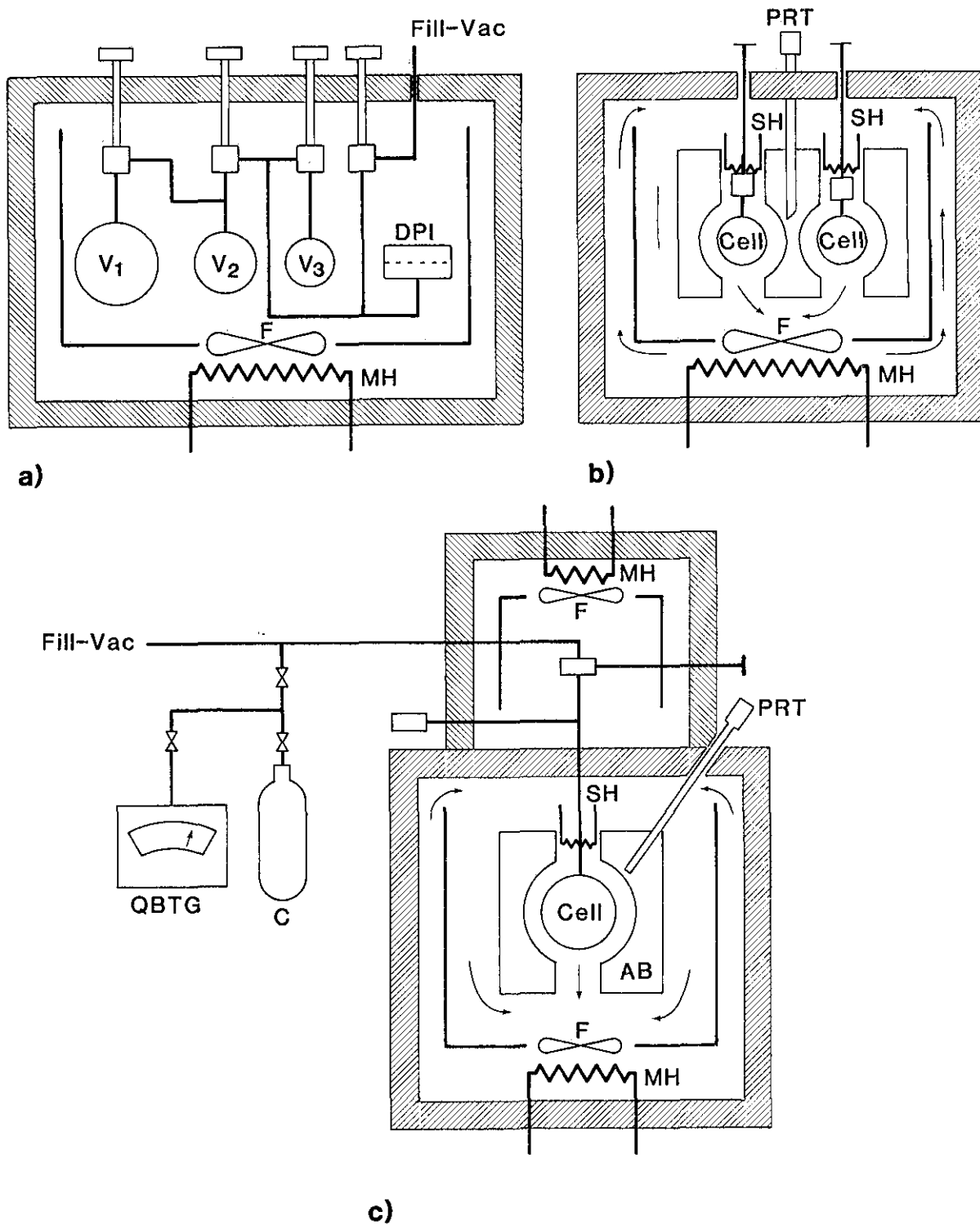


Figure 2—Schematic of the apparatuses. a) Burnett system showing cells, valving and piping. b) Burnett system showing the arrangement for temperature control. c) Isochoric system. In a), V_1 , V_2 , V_3 =three spherical cells and DPI=differential pressure transducer. In a), b), c), F=forced convection fan and MH=main heaters. In b) and c), SH=shim heaters, PRT=platinum resistance thermometer and AB=aluminum block. In c), QBTG=quartz bourdon tube gauge (pressure) and C=condensate cell.

heaters located in the air stream above each major component.

By means of diaphragm type differential pressure transducers, pressures in the Burnett experiment are measured by referencing to oil pressure derived from an oil operated commercial pressure balance with a stated accuracy of 0.015%.

A spherical configuration was chosen for the cells to allow a more accurate calculation of the change in cell volumes with pressure. Each cell was constructed with an identical ratio of outside to inside diameter to provide maximum error cancellation in the calculated volume ratios.

The system employed for the isochoric measurements is illustrated in c) of figure 2. This system consists of a single spherical cell with nominal volume of 120 cm³, encased in an aluminum block and suspended from a second insulated platen. To change experiments the Burnett system is simply replaced in the oven by the isochoric system.

Since the isochoric measurements can be made up to the maximum temperature of 600 °C, it is necessary to locate the valve and the pressure transducer in a less hostile environment. The valve and piping are enclosed in a second oven, maintained at the temperature of the initial Burnett measurements, where the density has already been determined, to allow a more accurate correction to be made to the assigned densities along the isochores.

Pressures along the isochores are determined from the vibration frequency of a commercial 0–40 MPa quartz transducer, calibrated frequently against the primary dead weight pressure balance. The transducer is estimated to be accurate to better than 0.05% full scale. The pressure transducer is located outside of the ovens in an enclosure thermostated at 40 °C.

Volumes of the isochoric cell, piping, valve, and pressure transducer were calibrated by low pressure nitrogen gas expansions from a volume previously calibrated by water weighing. This procedure allows isochore densities to be determined by weighing the sample after a run and provides a completely independent check on the densities determined in the gas expansion measurements.

Temperatures in both experiments are measured by using a platinum resistance thermometer (PRT) calibrated on the IPTS-68 by the National Bureau of Standards. The PRT is used to measure the temperature of the aluminum block. Temperatures of the components are then calculated from the block temperature and from any small temperature differences existing between the block and the components as determined by suitably placed differential thermocouples.

In use, either apparatus is suspended from a supporting structure. A mechanism for manipulating the ovens to enclose the apparatus for an experimental run and to retract them to provide access to the components is provided. For safety reasons, when working with toxic materials, the support structure is enclosed in a manner similar to a ventilation hood and is continuously aspirated by an exhaust fan located on the laboratory roof.

Computer Control and Data Acquisition

A computer was used for both experiment control and data acquisition. The series of Burnett measurements necessarily involved manual valve and pressure balance manipulations. In this case, the computer functions primarily as a thermal controller to bring the various elements of the apparatus into thermal equilibrium at the same temperature. The PRT and thermocouples are interrogated under computer control at a programmed time interval, usually about 30–40 s, using a scanner of custom design. Scanner relays were purchased commercially and had a claimed thermal EMF of less than 0.02 μV. Potentials are measured with a DVM with nanovolt resolution. Primary thermometry is performed by taking the ratio of the potential across the PRT and the potential across a series connected standard resistance of 50 Ω, carrying a current of less than 0.001 A, using a single DVM for the measurement. Two ratio determinations are made for each temperature measurement with current reversed for each. Averaging the two measurements minimizes the errors due to residual thermal EMF and tends to cancel DVM zero offsets. Temperature differences between the various apparatus components, calculated by the computer from the measured differential thermocouple potentials, are used to activate the shimming heaters to bring all elements to the target temperature. In equilibrium, temperature differences are typically maintained to better than ±0.025 °C at 250 °C. Since corrections are made for these temperature differences in the data analysis, differences of as much as 0.1 °C are considered tolerable. Data are logged onto hard copy and cassette tape after equilibrium is achieved, as determined by the operator.

The *P-T* measurements along pseudo-isochores are performed almost completely under computer control. Only initial filling of the system and subsequent venting or weighing of the sample at the end of a run is required of the operator.

In operation, the computer selects the preprogrammed temperature, sets the oven temperature and then determines the block temperature, cell temperature, and the rate of approach of the cell to the

target temperature by interrogating the various thermocouples and the PRT at programmed intervals of about 30–40 s. When the cell temperature is within 0.1 °C of the target temperature, the computer establishes a holding mode where the temperature control is continuously refined. Temperatures normally oscillate only a few hundredths of a degree about the target temperature in this mode. After an equilibration time (usually one hour) the data are logged onto hard copy and cassette tape, but only if programmed limits of temperature deviation and temperature and pressure drift rates are satisfied. The experiment is automatically shut down after a preset maximum pressure or temperature is reached. The sample is then manually vented, or it can be condensed into a small cell maintained at liquid nitrogen temperature for subsequent weighing.

Isochoric runs on propane at temperatures up to 325 °C, taking 50–60 h to complete, were carried out completely without operator attention. An automatic dial-up smart MODEM is interfaced with the controlling computer and allows experimental progress to be monitored and controlled by telephone from any remote site using a portable terminal or personal computer. Experiments usually are run continuously including evenings and weekends.

Data Analysis

The usual Burnett experiment involves the expansion of the sample gas from an initial volume V_1 into a second evacuated volume V_2 . Pressures before and after the expansion are measured. After isolation of V_1 and evacuation of V_2 , the process is repeated successively to low pressure. For any particular expansion.

$$\frac{P_i}{P_{i+1}} = \frac{Z_i}{Z_{i+1}} N_i, \quad (1)$$

where P = pressure, $Z = \frac{P}{\rho RT}$, ρ = density and $N_i = \frac{V_1 + V_2}{V_1}$. It is assumed here that the temperatures of V_1 and V_2 are constant and identical and it is recognized that the volume ratio N_i is slightly pressure dependent.

A number of ways to analyze such data have been suggested [4–6]. One common way is to express the compressibility factor Z as some function of pressure

$$Z = F(P). \quad (2)$$

Least squares analysis can be applied to the experimental data using eq (1) to determine the volume ratio N_0 at zero pressure and the parameters of $F(P)$. If $F(P)$ is a virial equation the determined parameters can be identi-

fied with the virial coefficients provided that the range of the data falls within the region where the virial equation is valid and the proper number of terms have been retained in the virial series. Considerable attention has been devoted to the problem of how to determine the proper number of terms to retain in the virial expansion [4–6]. The object of this work, however, is to obtain densities. We avoid the problem of the virial coefficients and use $F(P)$ only as a fitting function. The method can usually be used with data up to a maximum pressure corresponding to a density somewhat less than the critical density. Densities for higher pressure points can be obtained from the lower pressure data using the cell constant since

$$\rho_i = (\rho_{i+1}) N_i. \quad (3)$$

Even though it is possible to obtain the cell constant N_0 from a single fit to the experimental data, it is common, and often more accurate, to obtain it from a separate calibration experiment using a highly ideal fluid, usually helium. Extrapolation of the pressure ratio P_i/P_{i+1} to zero pressure yields the volume ratio directly since Z is identically one at zero pressure. A major advantage of the Burnett technique is that it is not necessary to do extensive, individual volume calibrations on the system, since only the volume ratio, which can be obtained from the expansion data, is required for data analysis.

For this work, the analysis is complicated by the fact that small temperature differences are allowed to exist between the volume elements composing the system. Equation (1) becomes

$$\frac{P_i}{P_{i+1}} = \sum_{j=1}^n \frac{V_{i+1,j}}{V_{i1}} \frac{T_{i1}}{T_{i+1,j}} \frac{Z_{i1}}{Z_{i+1,j}}, \quad (4)$$

where the system is now considered to consist of n volume elements which include the primary volumes V_1 and V_2 plus the volumes of connecting piping, valves and pressure transducer all at slightly different temperatures. The particular volume element is identified by the second subscript while the first subscript indicates the particular expansion as before. In general it is no longer sufficient for accurate data analysis to know only the cell constant N_0 ; the magnitude of all volume elements must also be known individually as well as certain density derivatives of the state surface.

For this analysis, the concept of a cell constant is retained but now

$$N_0 = \sum_{j=1}^n \frac{V_{0,j}}{V_{0,1}}, \quad (5)$$

where the subscript 0 again indicates $P_i=0$ and all volume elements are at the target temperature T . The $V_{i,j}$ can be expressed in terms of the $V_{0,j}$ as

$$V_{i,j} = V_{0,j} (1 + \alpha \Delta T_{i,j}) (1 + \beta_j P_i), \quad (6)$$

where α =volume thermal expansion coefficient, β_j =pressure dilation coefficient for volume j and the $\Delta T_{i,j}=T_{i,j}-T$ are the deviations from the target temperature T . If the $\Delta T \ll T$ and recognizing the fact that

$$\lim_{P \rightarrow 0} \frac{(1 + \beta_j P_{i+1})}{(1 + \beta_j P_i)} \frac{Z_{i,1}}{Z_{i+1,j}} = 1, \quad (7)$$

eq (4) can be used to obtain, after some manipulation and small approximation,

$$N_0 \approx \lim_{P \rightarrow 0} (1 + \alpha \Delta T_{i,1}) \frac{T}{T_{i,1}} \frac{P_i}{P_{i+1}} + \left(\frac{1}{T} - \alpha\right) \sum_{j=1}^n \frac{V_{0,j}}{V_{0,1}} \Delta T_{i+1,j}. \quad (8)$$

Equation (8) is used to obtain the cell constant N_0 using calibration data measured with helium. The first term on the right contains measured quantities. The second term is of order $10^{-4} N_0$ which allows the use of calculated values for the individual volume ratios ($V_{0,j}/V_{0,1}$) without introducing significant error in the value of N_0 obtained.

Using eq (6) in eq (4) the expression describing any expansion becomes

$$\frac{P_i}{P_{i+1}} = \frac{Z_{i,1} T_{i,1}}{1 + \alpha \Delta T_{i,1} + \beta_1 P_i} \sum_{j=1}^n \frac{V_{0,j}}{V_{0,1}} \left(\frac{1 + \beta_j P_{i+1} + \alpha \Delta T_{i+1,j}}{Z_{i+1,j} T_{i+1,j}} \right), \quad (9)$$

where the very small terms in $\alpha\beta$ have been omitted for clarity but which are included in the actual data reduction programs. For $\Delta T \ll T$ it is assumed that

$\frac{\partial Z_{i,j}}{\partial T_{i,j}} = \frac{\partial Z_i}{\partial T}$ and the compressibility factor Z_i at the target temperature T is related to $Z_{i,j}$ by

$$Z_{i,j} = Z_i \left[1 + \frac{1}{Z_i} \frac{\partial Z_i}{\partial T} \Big|_P \Delta T_{i,j} \right]. \quad (10)$$

Equation (9) can then be written, again after some manipulation, as

$$\frac{P_i}{P_{i+1}} = \frac{Z_i}{Z_{i+1}} \left[1 + \frac{1}{Z_i} \frac{\partial Z_i}{\partial T} \Big|_P \Delta T_{i,1} \right] \left(\frac{T_{i,1}}{T} \right) \left(\frac{A + P_{i+1} B + \alpha C}{1 + \beta_1 P_i + \alpha \Delta T_{i,1}} \right), \quad (11)$$

where

$$A = N_0 + \frac{1}{\rho_{i+1}} \frac{\partial \rho_{i+1}}{\partial T} \Big|_{P,j=1} \sum_{j=1}^n \frac{V_{0,j}}{V_{0,1}} \Delta T_{i+1,j}, \quad (12)$$

$$B = \sum_{j=1}^n \frac{V_{0,j}}{V_{0,1}} \beta_j + \frac{1}{\rho_{i+1}} \frac{\partial \rho_{i+1}}{\partial T} \Big|_{P,j=1} \sum_{j=1}^n \frac{V_{0,j}}{V_{0,1}} \beta_j \Delta T_{i+1,j} \quad (13)$$

and

$$C = \sum_{j=1}^n \frac{V_{0,j}}{V_{0,1}} \Delta T_{i+1,j} + \frac{1}{\rho_{i+1}} \frac{\partial \rho_{i+1}}{\partial T} \Big|_{P,j=1} \sum_{j=1}^n \frac{V_{0,j}}{V_{0,1}} \Delta T_{i+1,j}^2. \quad (14)$$

For $\Delta T=0$ this reduces to the isothermal Burnett situation. The N_0 in eq (12) is the largest term and is determined from the helium calibration runs. The remaining terms in (12), (13) and (14) are of order $10^{-4} N_0$ or smaller and are treated as small correction terms for which calculated values of the ($V_{0,j}/V_{0,1}$) are again used and for which it is sufficient to use only approximate values for the derivatives. Taking the logarithm of (11) to get

$$\ln P_i - \ln P_{i+1} = \ln Z_i - \ln Z_{i+1} + \ln N_0 + [\text{corrections} < 10^{-4}] \quad (15)$$

yields the working equation which was used, together with eq (2) in the analysis of the lower pressure Burnett data. Densities at the higher pressures in the Burnett measurements are obtained from the lower pressure densities of that run using the analogue of eq (3), which for this apparatus becomes

$$\rho_i = \rho_{i+1} N'_i, \quad (16)$$

where N'_i is an effective volume ratio given by

$$N'_i = \frac{N_i + \frac{1}{\rho_{i+1}} \frac{\partial \rho_{i+1}}{\partial T} \Big|_{P,i=1} \sum_{i=1}^n \frac{V_{i+1,i}}{V_{i,1}} \Delta T_{i+1,j}}{1 + \frac{1}{\rho_i} \frac{\partial \rho_i}{\partial T} \Big|_P \Delta T_{i,1}}. \quad (17)$$

Data for Propane

Numerous PVT data for propane up to 325 °C have been published. To verify the performance of the apparatus and to confirm the accuracy of the data analysis, limited measurements on propane to 325 °C have been made and have been compared with the literature values. Propane samples were research grade certified to be of 99.99% purity.

The two largest cell volumes were used for the expansions. Four expansion runs at 250 °C using helium were first made from a maximum pressure of about 5 MPa to a minimum pressure of about 0.13 MPa in order to derive the cell constant N_0 . A value of $N_0 = 1.60702 \pm .0001$ resulted from the analysis of pressure ratios using eq (8) and this value was used in the propane analysis.

Three expansions runs on propane at 250 °C, consis-

ting of a total of 30 pressure observations, were made [7]. Pressures ranged from a maximum of about 35 MPa, corresponding to a density of about 1.6 times the critical density, to a minimum of about 0.14 MPa.

The data are separated into two groups for analysis. At lower pressures, corresponding to densities less than the critical density, the data from all runs could be analyzed simultaneously using an expression for the compressibility Z in terms of pressure [8]. Since it is the nature of Burnett experiments to concentrate the data at the lower pressures, only the highest pressure point on each run could not be handled in this manner.

For data below 17 MPa the compressibility factor Z was represented as

$$Z = 1 + \sum_{i=1}^n B_i \left(\frac{P}{P_0} \right)^i \quad (18)$$

where $P_0 = 17$ MPa and was used with eq (15) for fitting purposes. Data were fitted, in the sense of least squares, by minimization of the difference between the left and right sides of eq (15). For pressures below 1.3 MPa, differences were weighted by P^{-1} to reflect the decreasing relative accuracy of the pressure balance at the lower pressures [8]. Other data were assigned a weight of 1. However, the results of the fit were insensitive to the weighting. For simplicity, derivatives appearing in the small correction terms of eq (15) were evaluated from a recently formulated correlation of propane data [9]. In the absence of derivative data, however, an iterative procedure can be used with equally good results. In this case a best estimate of the derivatives, based on a corresponding states approach, for example, could be used, or the correction terms could be ignored in first approximation. At the completion of the experiments, when the isochoric data are available, the derivatives can be estimated and successive iterations performed. Coefficients for eq (18) are shown in table 1. Burnett density results are tabulated in table 2 along with the densities obtained gravimetrically during the isochoric measurements.

It must be emphasized that eq (18) is simply a fitting function, and its coefficients cannot be identified with the virial coefficients, although the coefficient of the

Table 1. Coefficients of equation (18).

B_1	$= -4.14084758401E-01$
B_2	$= 0$
B_3	$= 0$
B_4	$= 4.01931812102E-01$
B_5	$= -2.20024107867E-01$
B_6	$= 9.14412474575E-03$
B_7	$= 4.22392090629E-02$

Table 2. Densities along the 250 °C isotherm obtained from the Burnett measurements and gravimetrically (the latter marked with*).

P (MPa)	ρ (mol/dm ³)	P (MPa)	ρ (mol/dm ³)
34.614	7.857	3.712	0.937
33.953	7.784*	3.501	0.879
28.960	7.241*	2.962	0.734
25.118	6.714*	2.390	0.583
22.311	6.252	2.250	0.547
20.322	5.864	1.894	0.456
20.277	5.843*	1.521	0.363
16.261	4.891	1.430	0.341
12.922	3.891	1.200	0.284
12.719	3.827*	0.960	0.226
12.185	3.649	0.902	0.212
10.384	3.044	0.755	0.177
8.536	2.421	0.603	0.141
8.083	2.271	0.566	0.132
6.922	1.895	0.473	0.110
5.674	1.507	0.354	0.082
5.364	1.413	0.221	0.051
4.566	1.179		

linear term is in reasonable agreement with published second virials for propane at 250 °C [10,11].

Densities for the highest pressures on each of the three runs were calculated from the next lower density of that run using eq (16).

Pressure measurements were made as a function of temperature at fixed total amounts of fluid using the isochoric system to extend the temperature range. Pressures were measured along 10 pseudo-isochores covering a density range of 1.7 to 7.7 mol/dm³. Observations were made at 10 °C intervals up to 150 °C and at 25 °C intervals up to 325 °C and to a maximum pressure of about 34 MPa. For isochores intersecting the 250 °C isotherm below 8.5 MPa the densities assigned to the pseudo-isochores were calculated from the intersection pressures using eq (18).

Since the data are concentrated at the lower pressures, the density data above 8.5 MPa were too widely spaced to permit accurate interpolation. To fill in these gaps several isochoric runs were terminated by condensing the samples into a cell held at liquid nitrogen temperature for the purpose of weighing. Sample weights were determined to better than ± 0.01 gram and densities at 250 °C were calculated using the volume calibration data for the isochoric system. Uncertainty in densities determined gravimetrically is estimated at better than $\pm 0.1\%$ due primarily to the uncertainty in volume calibrations. These densities are tabulated in table 2 along with the Burnett densities. Densities for pressures above 8.5 MPa, determined by both the Burnett and gravimetric methods, were used in a polynomial fit of pressure versus density, which in general represented

the densities to better than 0.05%. This function was used to calculate the densities assigned to the pseudo-isochores intersecting the 250 °C isotherm above 8.5 MPa.

In calculating the densities along the pseudo-isochores, corrections were made for fluid residing in the piping, valve, and the pressure transducer as well as for the effects of thermal expansion and pressure dilation of the cell. Data along the pseudo-isochores are presented in table 3.

Density data along several isotherms are compared with the literature data [11-14] in figure 3. Density deviations are plotted relative to an equation of state for propane [9] used as a baseline. This was done to eliminate the need for multiple interpolations when comparing data at slightly different temperatures. Absolute deviations in figure 3 reflect only the ability of the equation of state to reproduce the experimental data. Excellent agreement between data sets is indicated, however, by the fact that all the experimental data lie in a band of about $\pm 0.1\%$ which is well within the combined experimental errors. The excellent agreement between closely spaced densities along the 250 °C isotherm obtained in the Burnett measurements, the gravimetric measurements and from the literature data verify the performance of the experimental apparatus and confirm an estimated accuracy of about $\pm 0.1\%$ for the Burnett data.

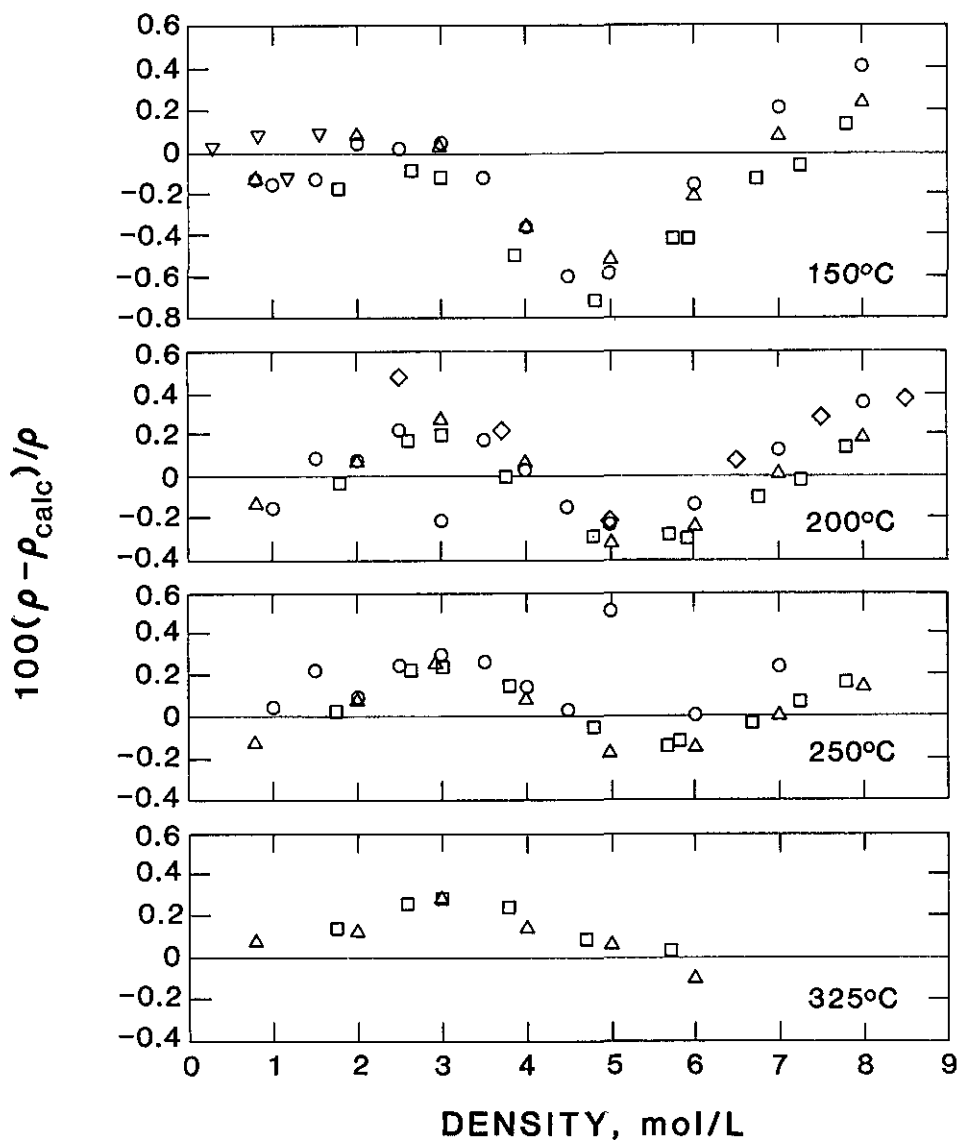
References

- [1] Burnett, E. S. Compressibility determinations without volume measurements. *J. Appl. Mech.* 3: A136; 1936.
- [2] Pope, G. A.; Patsy S. Chappelleav and Kiki Kobayashi. Virial coefficients of argon, methane and ethane at low reduced temperatures. *J. Chem. Phys.* 59: 423; 1973.
- [3] Only general operating characteristics are discussed. Lengthy descriptions of electronic instruments, logic circuitry and computer software have been omitted. It is this author's opinion that these elements, if not standard, are unique to a given apparatus and that each experimenter tends to develop these systems independently. More specific information can be obtained through personal communication.
- [4] Hall, K. R., and F. B. Canfield. Optimal recovery of virial coefficients from experimental compressibility data. *Physica* 33: 481; 1967.
- [5] Hall, K. R., and F. B. Canfield. A least-squares method for reduction of Burnett data to compressibility factors and virial coefficients. *Physica* 47: 99; 1970.
- [6] Wielopolski, P., and W. Warowny. A fast least-squares method for reduction of Burnett data to compressibility factors and virial coefficients. *Physica* 91A: 66; 1978.
- [7] Due to the many corrections that are made to the raw experimental data in the analysis, only analyzed data are given here. Raw data can be obtained from the author through personal communication.

Table 3. Propane densities along pseudo-isochores.

<i>P</i> (MPa)	<i>T</i> (°C)	ρ (mol/dm ³)	<i>P</i> (MPa)	<i>T</i> (°C)	ρ (mol/dm ³)
5.191	99.999	7.314	5.606	119.994	3.855
6.707	109.988	7.308	6.175	129.995	3.853
8.260	119.996	7.302	6.741	140.000	3.850
9.831	130.004	7.299	7.296	149.998	3.848
11.416	140.000	7.294	8.678	174.998	3.843
13.003	149.938	7.288	10.041	199.994	3.836
17.003	174.979	7.275	11.388	225.003	3.830
21.015	199.993	7.262	12.719	249.987	3.824
24.993	224.992	7.250	14.040	275.034	3.817
28.960	249.993	7.239	15.341	299.905	3.811
5.570	110.003	5.899	16.635	324.943	3.805
6.587	119.998	5.894	7.470	129.999	5.734
7.620	129.999	5.890	8.467	140.023	5.730
8.662	139.992	5.888	9.468	150.001	5.728
9.712	150.016	5.884	11.983	175.014	5.718
12.345	175.000	5.873	14.498	200.018	5.708
14.981	199.999	5.863	17.009	225.033	5.698
17.613	224.996	5.853	19.504	249.980	5.689
20.227	249.985	5.843	21.985	275.002	5.680
4.180	89.991	7.875	24.449	300.021	5.671
5.950	100.002	7.868	26.891	325.023	5.662
7.768	109.998	7.861	4.866	119.988	2.653
9.614	119.994	7.858	5.217	129.989	2.651
11.477	130.004	7.852	5.564	140.030	2.649
13.350	140.007	7.845	5.905	149.996	2.648
15.230	149.991	7.839	6.744	175.023	2.644
19.941	175.006	7.825	7.566	200.039	2.640
24.646	200.015	7.812	8.374	225.034	2.636
29.319	225.001	7.799	9.169	249.968	2.632
33.953	250.005	7.787	9.955	274.960	2.628
4.804	100.000	6.783	10.734	299.980	2.624
6.082	110.002	6.778	11.504	325.041	2.619
7.397	119.996	6.772	5.134	119.995	3.013
8.735	129.999	6.770	5.549	130.011	3.011
10.087	139.996	6.765	5.957	140.011	3.009
11.449	150.021	6.760	6.359	149.976	3.007
14.869	174.997	6.747	7.354	174.989	3.003
18.298	199.996	6.735	8.323	199.998	2.998
21.721	225.006	6.724	9.282	225.023	2.994
25.118	250.006	6.713	11.160	274.984	2.984
28.498	275.021	6.703	12.084	300.032	2.980
31.853	300.032	6.693	12.996	324.977	2.975
6.020	120.012	4.805	3.722	110.000	1.779
6.779	130.006	4.802	3.935	120.001	1.778
7.539	140.011	4.798	4.145	130.004	1.777
8.298	150.001	4.795	4.352	140.009	1.776
10.192	175.012	4.789	4.556	150.001	1.775
12.073	199.970	4.781	5.058	174.999	1.772
13.946	224.994	4.772	5.550	199.996	1.770
15.801	250.005	4.764	6.035	224.995	1.767
17.642	274.943	4.756	6.512	249.994	1.765
19.462	299.904	4.749	6.984	275.029	1.762
21.282	324.917	4.741	7.449	299.971	1.760
4.443	99.998	3.860	7.911	325.020	1.757
5.031	109.999	3.858			

Figure 3—Comparison of density data from various sources:
 this work, □
 Beattie (ref. 12), ○
 Thomas (ref. 11), △
 Warony (ref. 13), ▽
 Tiechman (ref. 14), ◇



- [8] Kell, G. S. Experimental error of the Burnett experiment. *Physica* 105A: 56; 1981.
- [9] Ely, J. F., and B. A. Younglove. Personal communication.
- [10] See, for example J. H. Dymond and E. B. Smith. *The Virial Coefficients of Pure Gases and Mixtures, A Critical Compilation*. Oxford: Clarendon Press; 1980.
- [11] Thomas, Raymond H. P., and Roland H. Harrison. Pressure-volume-temperature relations of propane. *J. Chem. Eng. Data* 27: 1; January 1982.
- [12] Beattie, J. A.; W. C. Kay and J. Kaminsky. The compressibility of, and an equation of state for, gaseous propane. *J. Am. Chem. Soc.* 59: 1589; 1937.
- [13] Warowny, W.; P. Wielopolski and J. Stecki. Compressibility factors and virial coefficients for propane, propene and their mixtures by the Burnett method. *Physica* 91A: 73; 1978.
- [14] Tiechman, J. Pressure-density-temperature measurements of liquid propane and benzene. Ph.D. dissertation: Ruhr University, Bochum; 1978.

Radio Propagation in a Coal Seam and the Inverse Problem

D. A. Hill

National Bureau of Standards Boulder, CO 80303

Accepted: July 17, 1984

The longwall method of mining in underground coal seams is very efficient in uniform seams, but coal seam anomalies can make the method unprofitable and unsafe. This paper describes the theoretical basis for detection of coal seam anomalies using medium frequency (MF) radio transmission over paths on the order of 200 m in length. The key to the method is the sensitivity of the attenuation rate of the coal seam mode of propagation to changes in the coal seam parameters, such as height or electrical conductivity. From a large number of transmission paths, the principles of tomography can be used to reconstruct an image of the seam.

Key words: attenuation rate; coal seam; geophysical tomography; linear equation inversion; loop antenna; medium frequency.

1. Introduction

Most coal seams are horizontally bedded deposits on the order of a few meters in thickness, and an ideal seam is fairly flat with little variation in thickness over a large region. In the longwall method of coal mining [1]¹, two horizontal parallel entries separated by approximately 150 m are driven in the coal seam. The coal between the two entries is then mined out as the "longwall" retreats. The longwall method is very efficient for uniform coal seams, but coal seam anomalies can make the method unprofitable and unsafe. A remote sensing method that could detect coal seam anomalies would be extremely useful.

Seismic methods are currently being explored in coal seams [2], but their effectiveness is as yet undemonstrated. Underground radars using VHF (30 MHz-300 MHz) have been used for some short-range applications, but they do not have sufficient range [3] to

probe the entire coal panel between the longwall entries. During the 1970s, it was found that communication between loop antennas using MF (300 kHz—3 MHz) was possible in coal seams for horizontal ranges up to several hundred meters [4,5]. The dominant mode of propagation at MF in coal seams is TM (transverse magnetic) with the magnetic field horizontally polarized. Because the electric field is primarily vertically polarized with only a small longitudinal component, the mode is nearly TEM (transverse electromagnetic) and is commonly referred to as the quasi-TEM mode or coal seam mode. And because the propagation constant of the quasi-TEM mode depends on the coal seam parameters (thickness and electrical properties), it should be a useful mode of propagation for remote probing of the coal seams.

This paper's purpose is to explore the theoretical feasibility of using MF radio transmission in remote sensing of coal seams, and its remaining sections are organized as follows. In section 2, the propagation constant and the field distribution are studied for a uniform coal seam. The dependence of the attenuation rate on the seam parameters is of particular importance. In section 3, the excitation of the TEM mode by a vertical loop (horizontal magnetic dipole) is analyzed. In section 4,

About the Author: D. A. Hill is an electronics engineer in NBS' Electromagnetic Fields Division.

¹Figures in brackets indicate literature references at the end of this paper.

transmission through a longwall coal panel is examined and the question of how to process the transmission data is explored. This is an area where further work is required. In section 5, conclusions are presented, and areas for further work are suggested.

2. Attenuation Rate and Field Distribution for the Quasi-TEM Mode

The geometry for a uniform coal seam is shown in figure 1. The seam has thickness $2h$, and the coal permittivity and conductivity are ϵ_c and σ_c respectively. The permittivity and conductivity of the surrounding rock are ϵ_r and σ_r respectively. Free space permeability μ_0 is assumed everywhere.

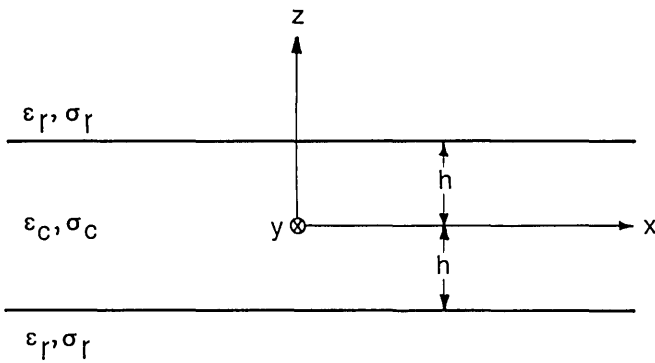


Figure 1—Geometry for a uniform coal seam of thickness $2h$.

The time dependence is $\exp(j\omega t)$, and it is suppressed throughout. The wavenumbers for the coal and rock, k_c and k_r , are given by

$$k_c = \omega \sqrt{\mu_0 \epsilon_{cc}} \quad \text{and} \quad k_r = \omega \sqrt{\mu_0 \epsilon_{rc}} \quad (1)$$

where $\epsilon_{cc} = \epsilon_c - j \sigma_c / \omega$

and $\epsilon_{rc} = \epsilon_r - j \sigma_r / \omega$.

The lowest order mode is transverse magnetic (TM), and for propagation in the x direction it has only an H_y magnetic field component. The mode equation for this lowest order mode has been given elsewhere [6,7], but we will derive it here because we need the resultant field expressions in the coal and in the rock. H_y must satisfy the following Helmholtz equation:

$$(\nabla^2 + k_c^2)H_y = 0, \quad |z| < h$$

$$(\nabla^2 + k_r^2)H_y = 0, \quad |z| > h. \quad (2)$$

The lowest order mode is even in z , and we also require that H_y is propagating in the x direction and satisfies eq (2). Thus we can write H_y in the coal ($|z| < h$) in the following form:

$$H_y = H_0 \exp(-j k_c S x) \cos(k_c C z), \quad (3)$$

where $S^2 + C^2 = 1$.

H_0 is an arbitrary constant, and S is a normalized propagation constant which must be determined from the mode equation. The fields are independent of y , and the x and z components of the electric field, E_x and E_z , are given by the following for $|z| < h$:

$$E_x = \frac{-1}{j \omega \epsilon_{cc}} \frac{\partial H_y}{\partial z} \quad \text{and} \quad E_z = \frac{1}{j \omega \epsilon_{cc}} \frac{\partial H_y}{\partial x}. \quad (4)$$

Substituting eq (3) into eq (4), we obtain the following expressions for E_x and E_z :

$$\begin{aligned} E_x &= -j C \eta_c H_0 \exp(-j k_c S x) \sin(k_c C z), \\ E_z &= -S \eta_c H_0 \exp(-j k_c S x) \cos(k_c C z), \end{aligned} \quad (5)$$

where $\eta_c = \sqrt{\mu_0 / \epsilon_{cc}}$.

For $z > h$, H_y must satisfy the Helmholtz equation in eq (2). Also we require that H_y must decay as z goes to positive infinity. An appropriate form for H_y for $z > h$ is

$$H_y = A \exp(-j k_c S x) \exp(-j u z), \quad (6)$$

where $u = \sqrt{k_r^2 - k_c^2 S^2}$

and $\text{Im}(u) < 0$.

A is an unknown constant, and Im denotes imaginary part. E_x and E_z are again determined from Maxwell's curl equation:

$$\begin{aligned} E_x &= \frac{-1}{j \omega \epsilon_{rc}} \frac{\partial H_y}{\partial z} \\ &= \frac{uA}{\omega \epsilon_{rc}} \exp(-j k_c S x) \exp(-j u z) \end{aligned} \quad (7)$$

and

$$E_z = \frac{1}{j \omega \epsilon_{rc}} \frac{\partial H_y}{\partial x} = \frac{-k_c S A}{\omega \epsilon_{rc}} \exp(-j k_c S x) \exp(-j u z).$$

Similar expressions for H_y , E_x , and E_z can be obtained for $z < h$ from the fact that H_y and E_z are even in z and E_x is odd in z .

At $z = h$, H_y and E_x must be continuous which leads to the following pair of equations:

$$H_0 \cos(k_c C h) = A \exp(-j u h),$$

$$-j C \eta_c H_0 \sin(k_c C h) = \frac{u A}{\omega \epsilon_{rc}} \exp(-j u h). \quad (8)$$

From the first equation A can be written

$$A = \frac{H_0 \cos(k_c C h)}{\exp(-j u h)}. \quad (9)$$

By substituting eq (9) into the second equation in eq (8), we obtain the following mode equation to be solved for C :

$$j k_c C \tanh(j k_c C h) + j u \epsilon_c / \epsilon_{rc} = 0. \quad (10)$$

Equation (10) is consistent with earlier results [6-8], and is in a form which is easy to solve numerically. The solution of eq (10) by Newton's method [9] is detailed in the Appendix.

The reason that coal seams support a quasi-TEM mode quite effectively is that the coal conductivity σ_c is normally much smaller than the rock conductivity σ_r [4,7]. The propagation constant Γ of the quasi-TEM mode is given by

$$\Gamma = j k_c S = j k_c \sqrt{1 - C^2}, \quad (11)$$

where $\text{Re}(\Gamma) > 0$,

C is determined from Appendix eq (A-3) and Re indicates the real part. The attenuation rate of the coal seam is the easiest quantity to obtain from transmission measurements, and is given by $8.686 \text{Re}(\Gamma)$ in dB/m. Additional information is available from the phase velocity of the quasi-TEM mode, but phase measurements have not been attempted in coal seams.

In figure 2 we show the attenuation rate of the quasi-TEM mode as a function of frequency for the following parameters:

$$\sigma_c = 10^{-4} \text{ S/m}, \quad \epsilon_c / \epsilon_0 = 6, \quad \sigma_r = 10^{-1} \text{ S/m}, \quad \epsilon_r / \epsilon_0 = 15, \quad \text{and} \quad 2h = 2\text{m}.$$

The permittivities are normalized to the free space value ϵ_0 . The computer code, written to generate the attenuation rate, was checked by comparing the results with those of Delogne [7], and in all cases agreed to graphical accuracy. As expected, the attenuation rate increases

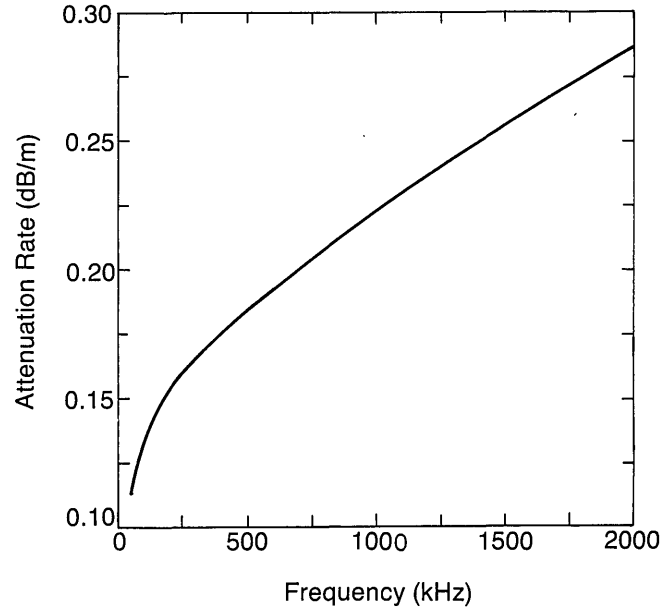


Figure 2—Attenuation rate as a function of frequency. Parameters: $\sigma_c = 10^{-4} \text{ S/m}$, $\epsilon_c / \epsilon_0 = 6$, $\sigma_r = 10^{-1} \text{ S/m}$, $\epsilon_r / \epsilon_0 = 15$, $2h = 2\text{m}$.

with frequency just as it does for a plane wave in an infinite rock medium. This indicates that the chosen frequency should be as low as possible to increase the range. However, there are two reasons for not choosing too low a frequency. For remote sensing, the resolution decreases as the frequency is decreased. Also, antenna efficiency decreases as the frequency is decreased. As a result of the tradeoff between attenuation rate and antenna efficiency, the maximum communication range between loop antennas in a coal seam was obtained for frequencies on the order of 500 kHz [5].

In figures 3-5, we show the attenuation rate as a function of various seam parameters for a frequency of 500 kHz. Since the goal is to detect changes in seam parameters from measurements of attenuation rate, it is desirable for the attenuation rate to be sensitive to changes in the seam parameters. The most important thing to detect in practical applications is a decrease in seam thickness $2h$. Figure 3 shows that the attenuation rate increases rapidly as thickness decreases below 1 m. This qualitative behavior can be predicted from Appendix eq (A-6). In figure 4 the attenuation rate is seen to increase as coal conductivity σ_c increases for both a plane wave and the quasi-TEM mode. The behavior of the attenuation rate as a function of rock conductivity σ_r is more complicated, as shown in figure 5. For large σ_r , the wall loss decreases as σ_r is increased as indicated by the second term in Appendix eq (A-6). However, as σ_r becomes small, more of the energy propagates in the rock, and the attenuation rate decreases as σ_r decreases.

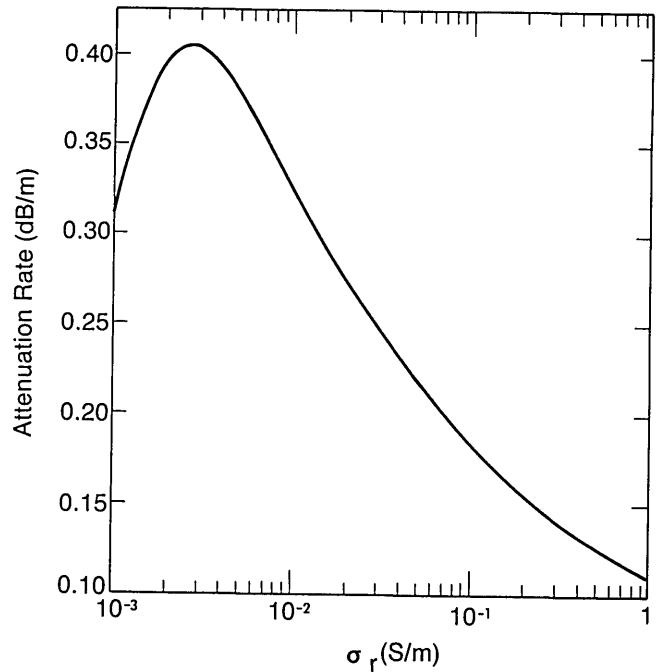
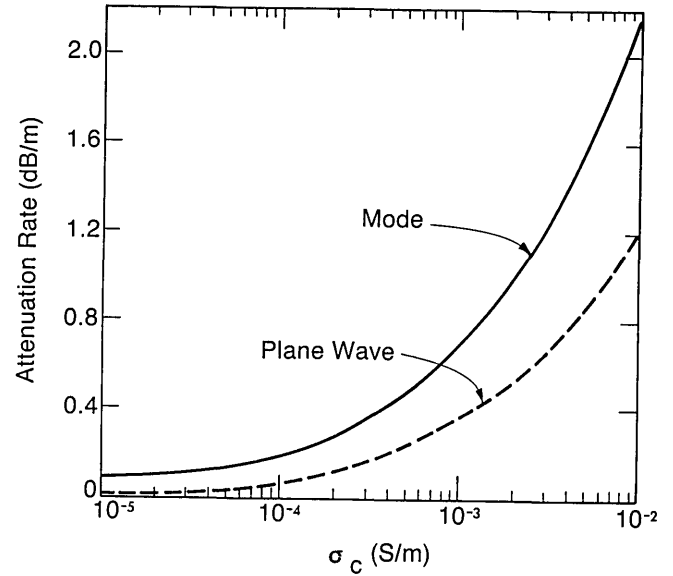
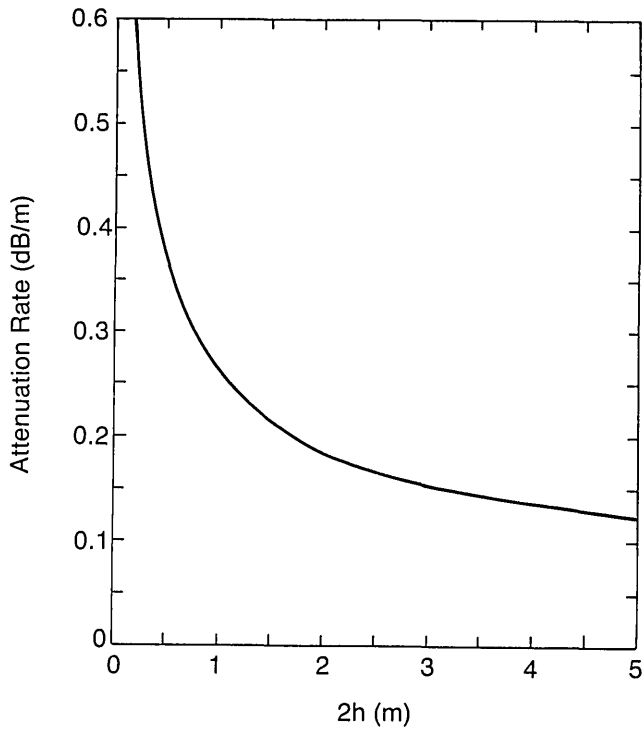


Figure 3-5—From above, clockwise: Attenuation rate as a function of seam thickness. Parameters: $f=500$ kHz, $\sigma_c=10^{-4}$ S/m, $\epsilon_c/\epsilon_0=6$, $\sigma_r=10^{-1}$ S/m, $\epsilon_r/\epsilon_0=15$. Next, attenuation rate for both a plane wave and the quasi-TEM mode as a function of coal conductivity. Parameters: $f=500$ kHz, $\epsilon_c/\epsilon_0=6$, $\sigma_r=10^{-1}$ S/m, $\epsilon_r/\epsilon_0=15$, $2h=2$ m. Finally, attenuation rate as a function of rock conductivity. Parameters: $f=500$ kHz, $\sigma_c=10^{-4}$ S/m, $\epsilon_c/\epsilon_0=6$, $\epsilon_r/\epsilon_0=15$, $2h=2$ m.

In figures 6-8 the electric and magnetic field distributions are shown for three different values of rock conductivity σ_r . The normalization field E_0 is the value of E_z at $z=0$ and is given by

$$E_0 = \eta_c S H_0. \quad (12)$$

All field components decay exponentially in the rock ($z > h$), and the decay rate is most rapid for the largest value of σ_r . Inside the coal seam, H_y and E_z are the dominant field components, and they are nearly constant in z . Thus a vertical electric dipole or a horizontal

magnetic dipole could be used to excite (or receive) the mode, and they would be insensitive to the vertical position. The horizontal electric field is zero at the center of the seam and is fairly small throughout the seam. Thus the mode is quasi-TEM. However, in the rock $|E_x|$ is larger than $|E_z|$ because E_z drops discontinuously to a small value in the rock. Thus the electric current flow is primarily horizontal in the rock. In addition to providing information on excitation of the quasi-TEM mode, the field distributions in figures 6-8 also indicate how anomalies in the seam will be illuminated.

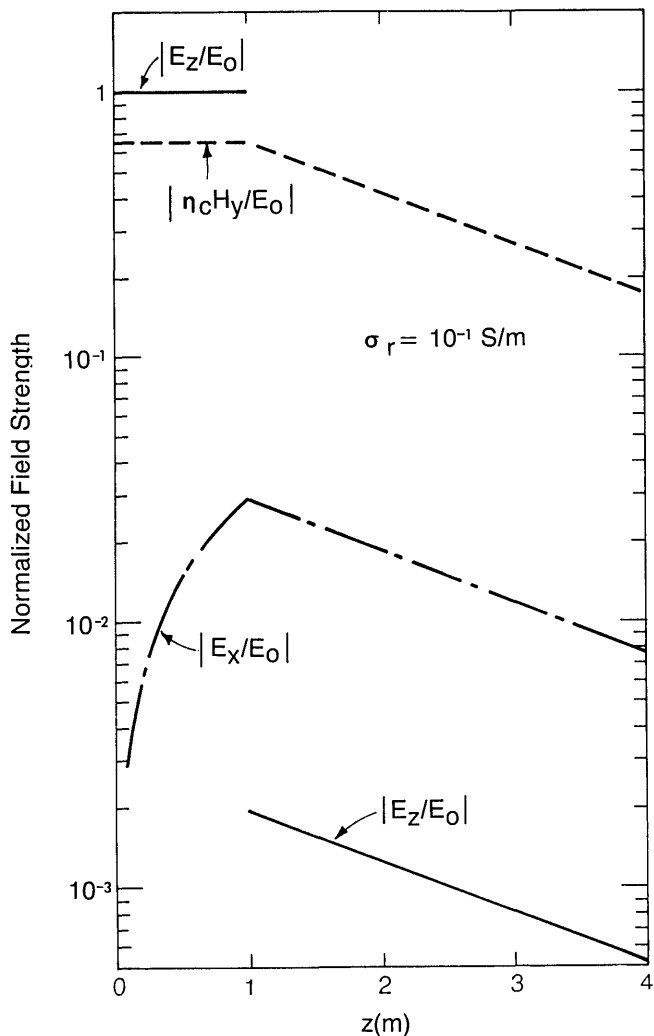


Figure 6—Electric and magnetic field distributions of the quasi-TEM mode. Parameters: $f=500$ kHz, $\sigma_c=10^{-4}$ S/m, $\epsilon_c/\epsilon_0=6$, $\sigma_r=10^{-1}$ S/m, $\epsilon_r/\epsilon_0=15$, $2h=2$ m.

3. Excitation of the Coal Seam Mode by a Vertical Loop Antenna

From the field distributions in figures 6–8, it is clear that either a vertical electric dipole or a horizontal magnetic dipole will be effective in exciting the quasi-TEM mode. Short electric dipoles (or monopoles) located in or near a conducting medium are generally inefficient because of near-field losses [10-12]. The near-field losses are generally smaller for magnetic dipoles or small loops [11,13], because the dominant near field is the quasi-static magnetic field. Consequently loop antennas have been considered best for communication in coal seams [4,5]. In this section we analyze the excitation of the quasi-TEM mode by a horizontal magnetic dipole (a small vertical loop with its axis horizontal).

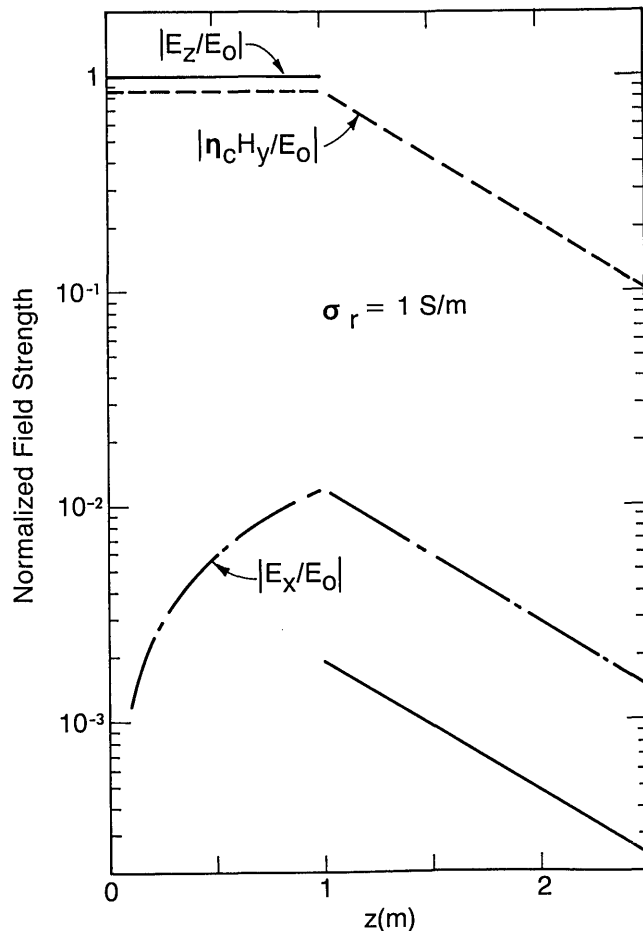


Figure 7—Electric and magnetic field distributions for a higher rock conductivity.

We consider a small loop of area A carrying a current I as shown in figure 9. The loop is centered on the z axis at $z=z_0$, and the loop axis is in the y direction. Thus the source can be considered a y -directed magnetic dipole of moment IA . This source radiates both a continuous spectrum of plane waves and a discrete spectrum of waveguide modes. For sufficiently large horizontal distances, the continuous spectrum can be ignored because it corresponds to highly attenuated waves traveling in the highly conducting rock walls. Also all higher order waveguide modes are highly attenuated because they are all well below cutoff. This is because $|k_c|2h$ is much less than unity at MF. Thus only the quasi-TEM mode which has no low frequency cutoff is significant at MF.

The excitation of the quasi-TEM mode has been considered by Delogne [7], and his result for the azimuthal component of the magnetic field H_ϕ is

$$H_\phi = \frac{k_c^2 I A}{2\pi h} \Lambda \cos(k_c C z) \cos(k_c C z_0) K_1(\Gamma\rho) \cos\phi,$$

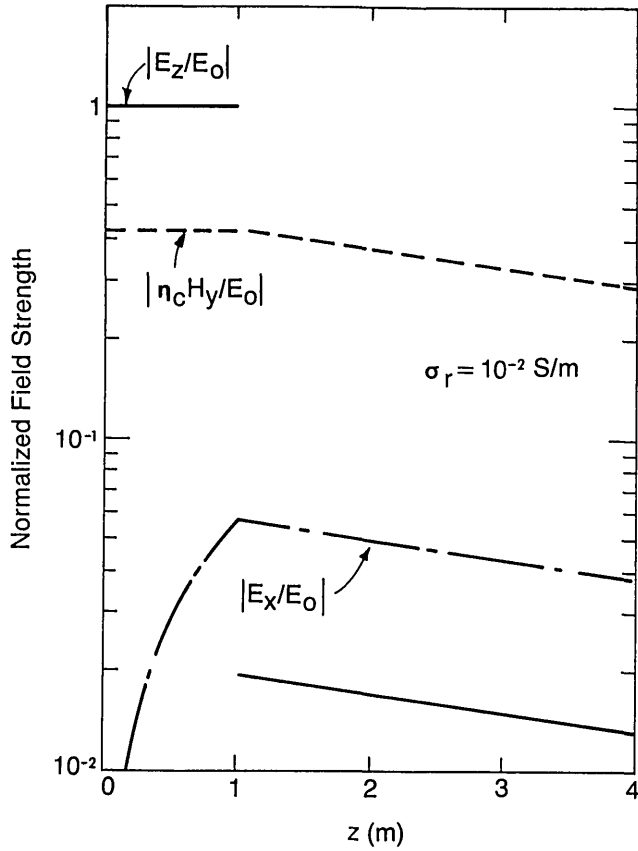


Figure 8—Field distribution for a lower rock conductivity.

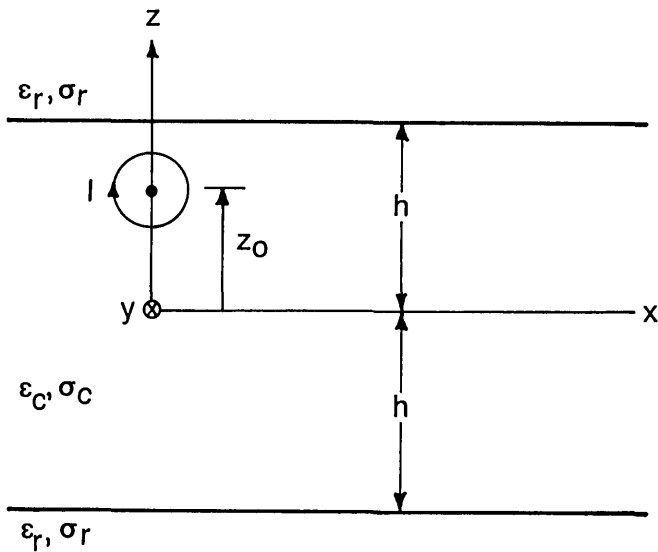


Figure 9—Vertical source loop (horizontal magnetic dipole) in a coal seam.

where $\cos \phi = \frac{x}{\rho}$, $\rho = \sqrt{x^2 + y^2}$, (13)

$$\Lambda = \left[1 + \frac{k_r^2 - k_c^2}{k_r^2 - k_c^2 C^2} \frac{\sin(k_c C 2h)}{(k_c C 2h)} \right]^{-1},$$

K_1 is a modified Bessel function [14], and C is determined from the solution of the mode eq (10). Equation (13) is valid when both the source and the field point are located in the coal seam ($|z| < h$ and $|z_0| < h$), and this is the usual case of interest. When $|\Gamma|\rho$ is large, we can replace $K_1(\Gamma\rho)$ by its asymptotic expansion [14]:

$$K_1(\Gamma\rho) \sim \sqrt{\frac{\pi}{2\Gamma\rho}} \exp(-\Gamma\rho). \quad (14)$$

Using eq (14), we can rewrite eq (13) as

$$H_\phi \sim H_i \frac{2\rho}{h} \sqrt{\frac{\pi}{2\Gamma\rho}} \Lambda \cos(k_c C z) \cos(h_c C z_0) \exp[-j k_c (S-1)\rho], \quad (15)$$

where

$$H_i = \frac{IA k_c^2}{4\pi\rho} \exp(-j k_c \rho) \cos \phi.$$

The reason for the normalization in eq (15) is that H_i is the far field of a magnetic dipole in an infinite coal medium for the case $z = z_0$. Note that the $\cos \phi$ factor leads to maximum in the plane of the loop ($y = 0$) and nulls along the loop axis ($x = 0$). The remaining factors yield the effect of the surrounding rock walls. The first factors involving ρ and h indicate that the coal seam mode has cylindrical spreading whereas H_i has spherical spreading. Λ relates to the excitation of the mode. The two cosine factors are the “height-gain” factors for the source and the observer within the seam. The exponential factor arises because the propagation constant of the mode is not the same as that of the infinite coal medium.

For the case where the rock conductivity is much greater than the coal conductivity ($|k_r| \gg |k_c|$), the expression in eq (15) simplifies considerably. In this case, C and S are given approximately by Appendix eqs (A-5) and (A-6):

$$C \approx \sqrt{\frac{j}{k_r h}} \text{ and } S \approx 1 + \frac{1}{j2k_r h}. \quad (16)$$

Thus C is small, and S is close to unity. We assume that $k_c C h$ is small compared to unity, and thus the cosine factors are nearly unity:

$$\cos(k_c C z) \approx \cos(k_c C z_0) \approx 1. \quad (17)$$

This means that the height of the transmitter and receiver within the coal seam is not important, and this is consistent with the numerical results in figures 6-8. The exponential factor can be simplified from eq (16):

$$\exp [-j k_c (S-1)\rho] \approx \exp \left(\frac{-k_c \rho}{2 k_r h} \right). \quad (18)$$

The excess attenuation over that of an infinite coal medium is given by eq (18), and is seen to be inversely proportional to that coal seam thickness $2h$. This is an important result in remote sensing of the seam height. The remaining factors in eq (15) can also be simplified from eq (16), and the result for H_ϕ is

$$H_\phi \approx H_i \sqrt{\frac{\rho}{h}} \sqrt{\frac{\pi}{2j k_c h}} \exp \left(\frac{-k_c \rho}{2 k_r h} \right). \quad (19)$$

4. Interpretation of the Transmission Data

In longwall mining there are normally two parallel entries approximately 150 m apart, and these entries are accessible for radio transmission measurements. A logical measurement scheme is to step the transmitting and receiving loop antennas along the entries as shown in figure 10. If there are N transmitting and N receiving positions, then there are N^2 transmission measurements. The loops are assumed to have their axes in the y direction, and the received voltage v is proportional to H_x :

$$v = j \omega \mu_0 A_r H_x, \quad (20)$$

where $H_x = H_\phi \cos \phi$

and A_r is the area of the receiving loop.

There are many possible methods for interpreting the transmission data. Since the coal seam supports only a single mode at MF, the attenuation rate of the quasi-TEM mode is the most logical quantity to work with. If we assume that the coal seam parameters vary slowly, we can approximately neglect reflection and refraction and assume straight ray propagation as indicated in figure 10. In that case the magnitude of H_x for the i^{th} ray path can be approximately written:

$$|H_{xi}| \approx \frac{H_i \cos^2 \phi_i}{\sqrt{\rho_i}} \exp \left[-\int_0^{\rho_i} \alpha(x, y) d\rho \right], \quad (21)$$

where H_i is a constant depending on the transmitting antenna and the coal seam parameters, $\alpha(x, y)$ is the attenuation rate in nepers/m and depends on x and y , ρ_i is the length of the i^{th} ray, and ϕ_i is the angle of the i^{th} ray with the x axis. The form of eq (21) is justified from the theory for the uniform coal seam in the previous section.

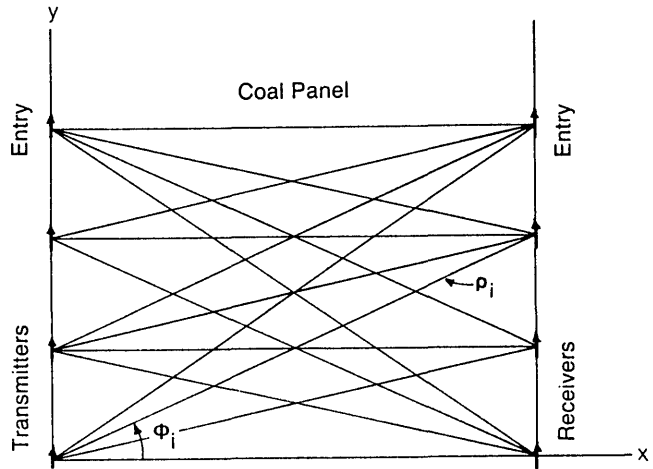


Figure 10—Top view of a longwall mine. The transmitting and receiving loops have their axes in the y direction and are moved along the parallel entries.

From eqs (20) and (21), the magnitude of the received voltage v_i for the i^{th} ray path can be written:

$$|v_i| \approx \frac{V_0 \cos^2 \phi_i}{\sqrt{\rho_i}} \exp \left[-\int_0^{\rho_i} \alpha(x, y) d\rho \right], \quad (22)$$

where V_0 is a constant which depends on both antennas and the seam parameters. Taking the logarithm of both sides of eq (22), we have

$$\int_0^{\rho_i} \alpha(x, y) d\rho = \ln \frac{V_0 \cos^2 \phi_i}{|v_i| \sqrt{\rho_i}}. \quad (23)$$

In geophysical tomography [15-17], the usual approach is to divide the intervening region into some large number of cells over which α is assumed to be constant. In that case the path integral in eq (23) can be reduced to a sum, and eq (23) can be written

$$\sum_l D_{il} X_l = Y_i, \quad (24)$$

where $Y_i = \ln \frac{V_0 \cos^2 \phi_i}{|v_i| \sqrt{\rho_i}}$,

X_l equals the unknown attenuation rate α for the l^{th} cell, D_{il} equals the length of the i^{th} ray through the l^{th} cell as

shown in figure 11, and $|v_i|$ is the magnitude of the measured voltage for the i^{th} ray path. Since eq (24) applies to all rays, the total system of equations can be written in the following matrix forms:

$$[D_{ii}] [X_i] = [Y_i]. \quad (25)$$

$[Y_i]$ is a column vector with N^2 elements corresponding to the N^2 transmission measurements in figure 10. The number of elements M in the unknown column matrix $[X_i]$ equals the number of cells, and normally M is chosen equal to or somewhat less than N^2 .

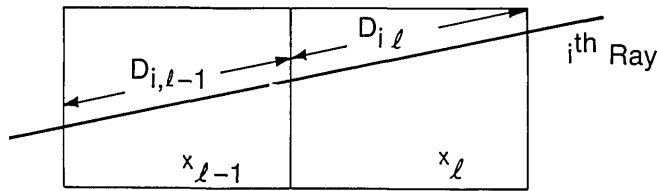


Figure 11—Geometry for the i^{th} ray. X_j is the attenuation rate in the j^{th} cell.

In theory $[X_i]$ could be determined from eq (25) by matrix inversion or pseudo-inversion:

$$[X_i] = [D_{ii}]^{-1} [Y_i], \quad M = N^2 \quad (26)$$

or

$$[X_i] = \left[[D_{ii}]^T [D_{ii}] \right]^{-1} [D_{ii}]^T [Y_i], \quad M > N^2,$$

where T indicates transpose.

In practice, the inversion of the linear equation in eq (25) has several difficulties. The values of $[Y_i]$ are not known exactly because $|v_i|$ contains noise and measurement error. Both the path integral model in eq (23) and the discrete version in eq (24) are approximate. Also, the system of equations in eq (25) may be very large. For example, if the antenna spacing is 5 m over a length of 150 m, then the number of equations is $30 \times 30 = 900$. In spite of these difficulties, there are numerous techniques which have been successfully applied to geophysical tomography problems [15-17]. Some of the popular methods and their acronyms are: algebraic reconstruction technique (ART) [18], simultaneous iterative reconstruction technique (SIRT) [19], and back projection technique (BPT) [20]. The description and application of these methods to geophysical tomography is well covered [16,17]. Since our system of equations for the coal seam geometry as described by eqs (24) and (25) is nearly identical to the equations for

cross-borehole probing [15-17], the past work on geophysical tomography is directly applicable. The two differences are that the coal seam mode experiences cylindrical spreading rather than spherical spreading and that the unknown is the attenuation rate of the coal seam mode rather than the bulk attenuation of the medium. The cylindrical spreading results in the $\rho_i^{-1/2}$ factor in eq (24) rather than ρ_i^{-1} for spherical spreading.

Since the solution of eq (25) for $[X_i]$ yields the attenuation rate α for the i^{th} cell, there is a further question of what seam parameters actually produced that value of α . The attenuation rate α is given by

$$\alpha = -\text{Im}(k_c S). \quad (27)$$

In general S depends on the seam parameters in a complicated manner via the mode eq (10). Even when the rock walls are highly conducting, α is fairly complicated:

$$\alpha \approx -\text{Im}(k_c) + \text{Re}\left(\frac{k_c}{2k_r h}\right). \quad (28)$$

Since α in eq (28) depends on three parameters (k_c , k_r , and h), we cannot determine the three parameters from α . However, in some cases additional geologic information might be available. For example if the rock and coal properties are known and constant, the seam height can be obtained from:

$$2h \approx \frac{\text{Re}(k_c/k_r)}{\alpha + \text{Im}(k_c)}. \quad (29)$$

If eq (28) is not valid, $2h$ can be obtained from a curve as in figure 3.

Even if it were not possible to determine the coal seam parameters, just the information that seam attenuation α changes in a region would be valuable to miners. Such a change would indicate that the seam is not uniform, and core drilling could be done in that area to provide further information. In fact, in many cases the full tomographic processing of the transmission data might be more complicated than necessary. In some cases, anomalous regions have been readily apparent from the measured data because the few rays which pass through the region have shown very high attenuation [21]. The anomalies have later been verified by drilling or mining into the anomalous region. High conductivity anomalies in copper mines have also been found by a similar ray analysis [22].

The conditions under which the straight ray tomographic approximation is valid have been discussed by Dines and Lytle [16], and similar conditions apply here if we replace the wavelength by guide wavelength and

the skin depth by the 1/e distance for the mode. Then the conditions become [16]:

$$\rho_i > \frac{1}{\operatorname{Re}(S k_c)}, \text{ for all } i,$$

$$\text{and } -2 \operatorname{Im}(S k_c) < \operatorname{Re}(S k_c). \quad (30)$$

The first condition is well satisfied at 500 kHz for $\rho_i > 100$ m. The second condition is only marginally satisfied at 500 kHz, but is better satisfied when either the frequency or the coal dielectric constant ϵ_c is increased. Even when eq (30) is satisfied, it is also necessary that the seam parameters vary slowly in order that the straight ray approximation is valid. Otherwise reflection and refraction occur, and they can be included, but only with significant increase in complexity [23]. When scattering becomes very important, even further changes in the processing are required [24], and in some cases it is useful to search for the scattering pattern of expected anomalies [25]. More experience with coal seam anomalies is necessary to determine the best method for processing data. There is also the possibility that phase information could be useful.

5. Conclusions

The feasibility of using the quasi-TEM mode at MF for remote sensing of coal seams has been studied. The mode has sufficient range for transmission between longwall entries which are normally separated by about 150 m. The attenuation rate is sensitive to the coal seam parameters (coal conductivity, rock conductivity, and seam thickness), as shown in figures 3–5. Thus the mode should be useful in sensing variations in these parameters. The mode can be excited efficiently by a vertical electric dipole or a vertical loop (horizontal magnetic dipole).

Transmission between vertical loops located in the two entries appears to be a useful method for probing the coal seam. Because a coal seam supports only a single mode which is nearly TEM, the system of linear equations to be solved is nearly identical to the system of equations in geophysical tomography. Thus the work which has been done on geophysical tomography for cross-borehole probing is directly applicable to the probing of coal seams. In some cases, such as a fault or washout of the seam, the seam properties change rapidly, and tomography is not valid; strong scattering and reflection occur, and some other type of processing is required. However, the transmission measurements will still show that the seam is not uniform, and this information might be sufficient for practical mining applica-

tions. The same difficulties occur for other geophysical tomography applications when strong scattering is present in either electromagnetic or seismic cases [25].

The author would like to thank Dr. Larry G. Stolarczyk for suggesting the use of MF radio transmission for remote sensing of coal seams.

References

- [1] Murphy, J. N. and H. E. Parkinson. Underground mine communications. Proc. IEEE **66**: 26-50; 1978.
- [2] Buchanan, D. J.; P. J. Jackson and R. Davis. Attenuation and anisotropy in coal seams. Geophys. **48**: 133-147; 1983.
- [3] Cook, J. C. Radar transparencies of mine and tunnel rocks. Geophys. **40**: 865-885; 1975.
- [4] Emslie, A. G. and R. L. Lagace. Propagation of low and medium frequency radio waves in a coal seam. Radio Sci. **11**: 253-261; 1976.
- [5] Cory, T. S. Wireless radio transmission at medium frequencies in underground coal mines. Summary of measurements and expected system propagational effects. Workshop on Electromagnetic Guided Waves in Mine Environments: Boulder, CO; 1978.
- [6] Wait, J. R. Note on the theory of transmission of electromagnetic waves in a coal seam. Radio Sci. **11**: 263-265; 1976.
- [7] Delogne, P. *Leaky Feeders and Subsurface Radio Communication*. Stevanage, UK: Peter Perigrinus Ltd.; 1982, Sec. 2.6.
- [8] Wait, J. R. *Electromagnetic Waves in Stratified Media*, 2nd ed. New York: Pergamon Press; 1970, Ch. VI.
- [9] Hamming, R. W. *Numerical Methods for Scientists and Engineers*. New York: McGraw-Hill; 1973, Ch. I.
- [10] Wait, J. R. Impedance characteristics of electric dipoles over a conducting half-space. Radio Sci. **4**: 971-975; 1969.
- [11] Wait, J. R. and D. A. Hill. Impedance of an electric dipole located in a cylindrical cavity in a dissipative medium. Applied Phys. **11**: 351-356, 1976.
- [12] Hill, D. A. and J. R. Wait. The impedance of dipoles in a circular tunnel with an axial conductor. IEEE Trans. Geosci. Electron. **GE-16**: 118-126; 1978.
- [13] Wait, J. R. and K. P. Spies. A note on the insulated loop antenna immersed in a conducting medium. Radio Sci. J. Res. NBS **68D**: 1249-1250; 1964.
- [14] Abramowitz, M. and I. A. Stegun, Eds. Handbook of mathematical functions. Natl. Bur. Stand. (U.S.) Handbook; 1964.
- [15] Lager, D. L. and R. J. Lytle. Determining a subsurface electromagnetic profile from high-frequency measurements by applying reconstruction technique algorithms. Radio Sci. **12**: 249-260; 1977.
- [16] Dines, K. A. and R. J. Lytle. Computerized geophysical tomography. Proc. IEEE **67**: 1065-1073; 1979.
- [17] Radcliff, R. D. and C. A. Balonis. Reconstruction algorithms for geophysical applications in noisy environments. Proc. IEEE **67**: 1060-1064; 1979.
- [18] Gordon, R. A tutorial on ART (algebraic reconstruction techniques). IEEE Trans. Nucl. Sci. **NS-21**: 78-93; 1974.

- [19] Gilbert, P. Iterative methods for the three-dimensional reconstruction of an object from projections. *J. Theor. Biol.* **36**: 105-117; 1972.
- [20] Kuhl, D. E. and R. Q. Edwards. Image separation radioisotope scanning. *Radiology* **80**: 653-662; 1963.
- [21] Stolarczyk, L. G. Private communication; 1984.
- [22] Rao, V. M. and I. B. R. Rao. The radio wave absorption technique in Mailaram copper mines, India. *Geophys.* **48**: 391-395; 1983.
- [23] Radcliff, R. D. and C. A. Balanis. Electromagnetic geophysical imaging incorporating refraction and reflection. *IEEE Trans. Antennas Propagat.* **AP-29**: 288-292; 1981.
- [24] Devaney, A. J. Geophysical diffraction tomography. *IEEE Trans. Geosci. Remote Sensing* **GE-22**: 3-13; 1984.
- [25] Lytle, R. J.; E. F. Laine; D. L. Lager and D. T. Davis. Cross-borehole electromagnetic probing to locate high-contrast anomalies. *Geophys.* **44**: 1667-1676; 1979.

Appendix—Solution of Mode Equation

To solve eq (10) by Newton's method, we first define the function $f(C)$:

$$f(C) = j k_c C \tanh(j k_c C h) + \left(\frac{\epsilon_{cc}}{\epsilon_{rc}}\right) \sqrt{k_r^2 - k_c^2 (1 - C^2)}. \quad (\text{A-1})$$

The derivative of $f(C)$ with respect to C is

$$f'(C) = \frac{\partial f}{\partial C} = j k_c \tanh(j k_c C h) - k_c^2 C h \operatorname{sech}^2(j k_c C h) + j (\epsilon_c / \epsilon_r) k_c^2 C / \sqrt{k_r^2 - k_c^2 (1 - C^2)}. \quad (\text{A-2})$$

If C_n is an n^{th} estimate of the solution to $f(C) = 0$, then by Newton's method [8] the $n + 1$ estimate is

$$C_{n+1} = C_n - \frac{f(C_n)}{f'(C_n)}. \quad (\text{A-3})$$

The iteration in eq (A-3) is continued until the change in C is sufficiently small.

An initial estimate C_0 can be obtained by considering the perfectly conducting parallel plate case ($\epsilon_{rc} = \infty$). In this case, the second term in eq (A-1) is zero, and the solution is $C_0 = 0$. For large $\epsilon_{rc} / \epsilon_{cc}$, C_0 is not zero, but it is still small. Thus we can replace the tanh function by its argument:

$$j k_c C_0 (j k_c C_0 h) + j k_n \epsilon_{cc} / \epsilon_{rc} \approx 0. \quad (\text{A-4})$$

The solution to eq (A-3) is

$$C_0 \approx \sqrt{\frac{J}{k_r h}}. \quad (\text{A-5})$$

Equation (A-5) is consistent with an earlier result from Wait [8], and we use it for our initial estimate in eq (A-3). Equation (A-5) can also be used to obtain an approximate propagation constant of the mode:

$$j k_c S \approx j k_c \sqrt{1 - C_0^2} \approx j k_c \left(1 - \frac{1}{2} C_0^2\right) \approx j k_c + \frac{k_c}{2 k_r h}. \quad (\text{A-6})$$

The first term $j k_c$ is the propagation constant of a plane wave in an infinite coal medium, and the second term is a correction to account for the finite conductivity of the surrounding rock.

A Report on the National Bureau of Standards pH Standards

Y. C. Wu, W. F. Koch, and G. Marinenko

National Bureau of Standards, Gaithersburg, MD 20899

Accepted: September 19, 1984

In 1980, the research program in pH was re-established at the National Bureau of Standards (NBS). This report describes the state of this research, as well as the state of the NBS pH standards. The thermodynamic definition and the determination of pH are elaborated. The problems of liquid junction potentials encountered in the practical determination of pH are discussed. The goal of the research program in pH is to develop and maintain a unified pH scale based on clearly stated thermodynamic criteria, with a wide range of applicability to practical pH measurements.

Key words: activity; activity coefficient; buffers; galvanic cell; glass electrode; hydrogen ion; liquid junction; pH; silver/silver chloride electrode; Standard Reference Materials; standards; thermodynamics.

1. Introduction

The negative logarithm of the hydrogen ion activity is commonly known as pH [1]¹. This term is associated with the effective concentration of hydrogen ion. The importance of this quantity lies in the fact that it is the measure of the chemical reactivity of the acid and alkali in aqueous solutions. It is used extensively in monitoring agricultural and industrial processes. Functionally, pH lies at the base of many chemical synthetic processes and is essential in many analytical measurements. In biological and biochemical research, pH is important because it is fundamental to natural processes. In short, pH is intrinsic to life itself.

The determination of pH is based on physicochemical principles and can be performed by various techniques such as colorimetry, conductivity, and potentiometry.

About the Authors: All the authors are research chemists in the Inorganic Analytical Research Division of NBS' Center for Analytical Chemistry.

¹Numbers in brackets indicate literature references at the end of this paper. It should be noted here that the original definition was in terms of hydrogen ion concentration. It was S. P. L. Sorenson and K. Linderstrom-Lang (Compt. Rend. Trav. Carlsberg 15, 40, 1924) who first proposed hydrogen ion activity in the definition.

Of these, the potentiometric or the electromotive force (emf) method is the simplest, the most accurate, and hence the most widely used. This is particularly true since the invention and commercialization of the hydrogen ion sensitive glass electrode.

The employment of the glass electrode for determining pH generally requires the following arrangement:



where the single vertical bar is the electrode-solution interface and the double vertical bar is a liquid junction denoting an interface between the test solution and the salt bridge solution, the latter having an ion in common with the reference electrode. From the measured electromotive force of cell (I) the pH may be computed via the following equation:

$$\text{pH} \equiv \log a_{\text{H}} = \frac{E - (E_{\text{pH}}^{\circ} + E_{\text{j}})}{RT \ln 10 / F} = \frac{E - E_{\text{pH}}^{\circ'}}{k} \quad (1)$$

where a_{H} = the hydrogen ion activity (the charge, +, is dropped for convenience)

E = the observed emf of the cell

E_{pH}° = a constant, dependent on temperature and pressure and the types of electrodes used

- E_j = the liquid junction potential of the given cell
 R = the gas constant
 T = the kelvin temperature
 F = the faraday constant
 $k = (RT \ln 10)/F$
 $E_{\text{pH}}^{\circ'} = E_{\text{pH}}^{\circ} + E_j$

The last quantity, $E_{\text{pH}}^{\circ'}$, cannot be accurately evaluated. However if $E_{\text{pH}}^{\circ'}$ is assumed to be constant for a given system [2], and if a solution of known pH [pH(S)] is available, then the pH of an unknown solution [pH(X)] can be determined by using cell (I) twice: first with solution S, then with solution X and calculating the pH(X) from the difference in the respectively measured emf's as follows:

$$\text{pH(X)} = \text{pH(S)} + \frac{E_X - E_S}{k} \quad (2)$$

If pH(X) differs significantly from pH(S) or if the emf response of the system differs from the ideal Nernstian response of 1 pH unit per volt ($RT \ln 10/F$), then two pH standards (S1 and S2) should be used. The value of pH(X) can be computed according to eq (3):

$$\text{pH(X)} = \text{pH(S1)} + \frac{E_X - E_{S1}}{E_{S2} - E_{S1}} [\text{pH(S2)} - \text{pH(S1)}] \quad (3)$$

The choice of the two buffers S1 and S2 should be such that pH(X) falls between the values pH(S1) and pH(S2). Such is the practical determination of pH today.

Therefore, the availability of standard pH solutions is a necessary condition for the application of eq (2). Moreover, according to the application of Henderson's or Planck's equation for the approximation of the liquid junction potential, E_j [3-5], the standard pH solution should be made as similar to the test solution as possible with respect to pH and composition. Under such conditions the assumption regarding the constancy of $E_{\text{pH}}^{\circ'}$ is sound. Since in practice the conventional pH scale spans 14 pH units, several pH standards are required for establishing calibration points over the entire pH range.

In the United States, pH standards are promulgated and maintained by the National Bureau of Standards (NBS). Many foreign countries have also adopted the NBS approach to pH standardization. This work has been performed at NBS since the late 1930s [6] through the issuance of Standard Reference Materials. This approach, as well as the materials and values for the NBS pH buffer standards, have been accepted internationally. The theory and practices which are at the base of the certification process undergo periodic critical examination at NBS to remain current with new developments and technology and to be responsive to

changing and expanding national needs. A detailed discussion of the theory, the process, and the refinement of the evaluation and certification of pH standards at the NBS follows.

2. Thermodynamic Foundation of pH

The use of pH in the expression $\text{pH} = -\log a_{\text{H}}$ is purely a formalism because a_{H} , a single (hydrogen) ion activity, is indeterminate. The ultimate definition of pH should be made in terms of determinable quantities.

One way of determining the pH of a weak acid (HA) may be from the dissociation constant, K_a , of the acid, assuming K_a is known or can be independently determined:

$$K_a = \frac{a_{\text{H}} a_{\text{A}}}{a_{\text{HA}}} = \frac{a_{\text{H}} m_{\text{A}} \gamma_{\text{A}}}{m_{\text{HA}} \gamma_{\text{HA}}} \quad (4)$$

and

$$\text{pH} = \text{p}K_a + \log \frac{m_{\text{A}}}{m_{\text{HA}}} + \log \frac{\gamma_{\text{A}}}{\gamma_{\text{HA}}} \quad (5)$$

With the aid of the Debye-Hückel equation [7, 8]

$$\log \gamma_i = -AZ_i^2 \sqrt{I} / (1 + B \bar{a}_i \sqrt{I}) + bI \quad (6)$$

- where m = molality of the constituents
 γ_i = activity coefficient of the i th species
 $I = \frac{1}{2} \sum m_i Z_i^2$. (This is the definition of ionic strength only if the electrolyte is fully dissociated. Otherwise, the degree of dissociation, α , should be included. Thus $I = \frac{1}{2} \sum \alpha m_i Z_i^2$, e.g., I for 0.05 m potassium acid phthalate (KHP) at 25 °C is not 0.05 but 0.0533 [9].)
 Z_i = ionic charge of the i th ion
 A and B = constants dependent on the temperature and dielectric constant of the solvent
 \bar{a}_i = the ionic size
 b = an adjustable parameter

On the other hand, the pH of the same acid can be determined without the knowledge of K_a , using a galvanic cell without liquid junction, sometimes called the Harned cell:



The emf of this cell at one atmosphere (101.325 kPa) of hydrogen pressure is given by

$$E = E_{\text{Ag,AgCl}}^{\circ} - \frac{RT}{F} \ln m_{\text{H}} m_{\text{Cl}} \gamma_{\text{H}} \gamma_{\text{Cl}} \quad (7)$$

where m 's are molalities, γ 's the activity coefficients, R, T, F have their usual significance, and E is the measured emf. $E_{\text{Ag,AgCl}}^\circ$ is the potential of the silver-silver chloride electrode measured relative to the "standard hydrogen electrode," i.e.,



and

$$E = E_{\text{H}}^\circ - \frac{RT}{F} \ln \frac{a_{\text{H}^+}}{p_{\text{H}_2}^{1/2}} \quad (9)$$

where p is the pressure of the H_2 gas. When $p = p^\circ \equiv 1$, atmosphere and $a_{\text{H}^+} = a_{\text{H}^+}^\circ \equiv 1$, then, $E = E_{\text{H}}^\circ$. Since half-cell potentials cannot be measured independently, it has been established by convention that $E_{\text{H}}^\circ = 0$ at p_{H}° and at all temperatures. All other half-cell potentials are computed in relation to $E_{\text{H}}^\circ = 0$.

By putting all the known quantities together on the right hand side, eq (7) may be rewritten as

$$-\log a_{\text{H}}\gamma_{\text{Cl}} = \frac{E - E^\circ}{k} + \log m_{\text{Cl}} \quad (10)$$

Since by definition $\gamma_{\text{Cl}} = 1$ as m goes to zero, by plotting the right hand side of eq (10) vs m_{Cl} and extrapolating to $m_{\text{Cl}} = 0$, the limiting value of the acidity function can be expressed as $-\log(a_{\text{H}}\gamma_{\text{Cl}})_i^\circ$ [9]. This value corresponds to the acidity function at the particular ionic strength, I , of the weak acid HA and

$$\text{pH} = -\log(a_{\text{H}}\gamma_{\text{Cl}})_i^\circ + \log \gamma_{(\text{at } I)} \quad (11)$$

The last term of eq (11) may be evaluated from eq (6). Therefore, all the quantities related to pH, either from the dissociation constant or from the emf of galvanic cells without liquid junction, can be determined. Hence, within this framework the term pH is defined.

It should be noted that the application of eq (6) for the evaluation of the activity coefficients requires assumptions outside the domain of thermodynamics. However, it has been experimentally proved that this equation is a suitable approximation for the activity coefficient function of strong electrolytes up to 1 molal concentration [10,11] and therefore the use of this equation is justified for the determination of pH at ionic strength lower than 1 molal.

As the ionic strength decreases, the b -term in eq (6) becomes insignificant, and the influence of \hat{a}_i also decreases. By selecting a value for $B\hat{a}_i$ (for example 1.5, as recommended by the Bates-Guggenheim convention [12,13] at the ionic strength of around 0.1 molal), the resultant uncertainty in pH is less than 0.005 pH unit,

even if $B\hat{a}_i$ is varied by as much as 10%. The ionic strength of the standard pH solutions certified by NBS is ≤ 0.1 . Thus the Bates-Guggenheim convention,

$$\log \gamma_i = -\frac{Az_i\sqrt{I}}{1 + 1.5\sqrt{I}} \quad (12)$$

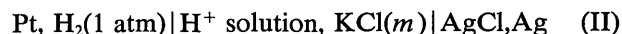
is justified within the present experimental uncertainty (see table 1), and is applicable to the certification of the NBS primary buffer standards.

New demands for pH standards of ionic strength greater than 0.1 molal, such as that for seawater, render the use of Bates-Guggenheim convention inapplicable. In these cases eq (6) must be used, and the values of \hat{a}_i and b must be determined experimentally.

3. NBS Standardization of pH Solutions

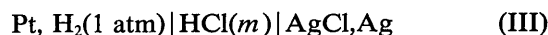
The standardization of pH solutions was initiated at NBS in the late 1930's when Hamer [14] suggested the use of a galvanic cell without a liquid junction, similar to cell II, for the purpose. Later Hamer and Acree [6] proved experimentally the applicability of cell II for the determination of pH. Early in the 1940's, Bates et al. [15] published a list of provisional pH values of standard buffers. In the following years the experimental setup and the treatment of data were significantly refined as the state of the art of measurement advanced.

The principle of the determination of pH and the thermodynamics of the establishment of a pH scale have been discussed in section 2. Because of the complexity of ionic interactions in electrolyte solutions, the knowledge of ionic activity or activity coefficients has been advanced little in recent years. The only improvements that have occurred in the determination of pH have been in the methods of measurement. Among various methods for determining pH, Hamer et al. [6,14] and later Bates [12,16] have ably demonstrated that a galvanic cell without a liquid junction,



is the best suited for the purpose. A detailed experimental account has been given by Durst [17].

Since eq (7) is used for the determination of pH, it is necessary to know $E_{\text{Ag,AgCl}}^\circ$. The value of $E_{\text{Ag,AgCl}}^\circ$ is determined, using the following cell [10]:



and the equation

$$E_{\text{Ag,AgCl}}^{\circ} = E_{\text{cell}} - E_{\text{H}}^{\circ} \quad (13)$$

where $E_{\text{H}}^{\circ} = 0$, under the conditions described in the previous section. However, the best values of E° reported for this cell disagree by 0.2 mV or more [18,19]. This indicates that not all silver-silver chloride electrodes behave identically. Therefore, for the most accurate pH work, the E° value of each individual Ag,AgCl electrode must be determined in cell III and the stability of each electrode firmly established before it may be used in cell II.

Using cell II, relying on thermodynamic principles, and by adopting the Bates-Guggenheim convention, the NBS has certified seven primary and three secondary pH standards. They are listed in table 1. The uncertainty associated with each of the primary standards is 0.005 pH and the uncertainty of the secondary standards is 0.01 pH.

The widespread use of cell I for practical pH measurements necessitates the use of pH standards that are traceable to the primary standards for calibration purposes. The work at NBS satisfies this need by providing definitively calibrated and certified pH standards.

The advantages and shortcomings of cell I have been discussed in section 1. Nevertheless, it is of interest to examine the data obtained with cell I by using a combination glass electrode to test the internal consistency of the NBS pH standards. The results are shown in table 2. The maximum deviation among all pH(S) listed in table 2 is 0.002 pH units. The NBS pH scale is internally consistent to at least that extent, thus confirming the usefulness of the approximations and conventions described in the first part of this report.

4. The Operational Determination of pH and the Problem of Liquid Junction.

The operational definition of pH entails the measurement of pH with cell I and the comparison of the pH of the unknown solution with that of the standard as shown in eq (2). Such comparison assumes the constancy of the liquid junction potential, E_j , in eq (1). This assumption has only limited validity. In some instances significant errors may be introduced in the pH determination by this assumption.

The problem of liquid junction potential has been the

Table 2. Internal consistency of the NBS pH scale.

Standard Solution	25 °C	ΔpH
1:1 Phosphate		
pH(S)	6.863	
pH(meas)	6.861	+0.002
Tartrate		
pH(S)	3.639	
pH(meas)	3.638	+0.001
Phthalate		
pH(S)	4.004	
pH(meas)	4.006	-0.002
Borax		
pH(S)	9.183	
pH(meas)	9.184	-0.001
Carbonate		
pH(S)	10.014	
pH(meas)	10.014	+0.000

Table 1. NBS pH Standards.

Solution composition (molality)	pH(S) at 25 °C	Temperature range (°C)	SRM
Primary Standards:*			
potassium hydrogen tartrate (satd. at 25 °C)	3.557	25 to 95	188
0.05 m potassium dihydrogen citrate	3.776	0 to 50	
0.05 m potassium acid phthalate	4.006	0 to 50	185f
0.025 m KH_2PO_4 + 0.025 m Na_2HPO_4	6.863	0 to 50	186Id/186IId
0.008695 m KH_2PO_4 + 0.03043 m Na_2HPO_4	7.410	0 to 50	186Id/186IId
0.01 m $\text{Na}_2\text{B}_4\text{O}_7 \cdot 10 \text{H}_2\text{O}$	9.180	0 to 50	187c
0.025 m NaHCO_3 + 0.025 m Na_2CO_3	10.010	0 to 50	191a/192a
Secondary Standards:**			
0.05 m potassium tetroxalate $\cdot 2\text{H}_2\text{O}$	1.679	0 to 95	189
0.01667 m tris*** + 0.05 m tris $\cdot \text{HCl}$	7.699	0 to 50	922/923
$\text{Ca}(\text{OH})_2$ (satd. at 25 °C)	12.454	0 to 60	

*Experimental uncertainty: ± 0.005 pH

**Experimental uncertainty: ± 0.01 pH

***tris: tris(hydroxymethyl)aminomethane.

subject of numerous studies [2,14,20,21] which indicate that the liquid junction potential is not a thermodynamic quantity, i.e., that the liquid junction potential, E_j , cannot be specifically defined. For example, E_j depends on the concentration of the salt bridge and on the temperature, but no functional correlation has been found. E_j also varies with specific electrolytes, such as strong and weak acids. Furthermore, it changes with the geometrical structure and the manner in which the junction of the salt bridge is formed [14,20]. Therefore, E_j cannot be determined exactly and eq (2) cannot be considered a rigorous thermodynamic definition of pH.

For the reasons outlined above, one cannot in general assume E_j to be constant in determining pH in solutions of unknown nature. It has been reported that the uncertainty in determining pH in acid rain [22] and in biological fluids [23], using a combination glass electrode in cell I, is significant, often as large as 0.5 pH.

5. Research on pH

An active research program in pH has been established at NBS to maintain the standards used for pH calibration, to respond to changing needs in this important determination, and to advance the science in tune with advances in chemical and electronic technology. This research effort includes both basic and applied studies and its diversity is illustrated by two projects now in progress.

Basic research is being conducted to establish firmly the standard potential (E°) of the Ag,AgCl electrochemical couple which is often used as the reference electrode in pH measurements. As alluded to in a previous section, there are variations in the measured E° of different preparations of Ag,AgCl electrodes. Recently, Bates [18] has reported that from over 30 independent measurements, values for E° of Ag,AgCl determined in cells without liquid junction vary from 0.2222 to 0.2228 V at 25 °C. The range is 0.0006 V, which amounts to differences of approximately 0.01 pH unit.

Variations in E° of such magnitude (0.6 mV) must be caused by the Ag,AgCl electrode itself, because the other factors in the system for determining E° can be systematically eliminated. In fact, experts decided in 1956 to assign an uncertainty of 0.2 mV to the E° measurements for this electrode [24]. The sources of problems associated with this electrode have been investigated by numerous workers in electrochemistry. The areas studied have included methodology, electrode preparation, and operational precautions. However, there is still need to define the characteristics of this electrode to reduce the uncertainties associated with pH measurements done on SRM's at NBS.

When classical experiments [19, wherein references cited] were repeated, it was observed that oxygen interacted with the electrode and was probably the major cause of the observed variations in E° . Although this observation was not new, the effect has never been fully discussed and investigated. To verify the effect of oxygen on the behavior of the electrode, we conducted the following experiments:

A. Electrode Preparation: A thermal electrolytic type of preparation was selected because the method is simple and results in an electrode with minimal (or least) contamination. Classical procedures were followed, except when electrodes were purposely exposed to either laboratory air or an argon atmosphere.

B. Cell EMF Measurement: The cell setup, temperature control, and measuring device were similar to those described by Durst [17] with minor modifications. Special care was taken to have the electrode and HCl solution under either laboratory air or an argon atmosphere. Measurements were made immediately after the preparation of the electrodes.

Four sets of experimental conditions were compared:

- | | |
|---------------------------------------|--|
| (a) $E_{\text{el(O)}} - \text{S(O)}$ | (c) $E_{\text{el(Ar)}} - \text{S(O)}$ |
| (b) $E_{\text{el(O)}} - \text{S(Ar)}$ | (d) $E_{\text{el(Ar)}} - \text{S(Ar)}$ |

where el(O)=electrode exposed to air, el(Ar)=electrode exposed to argon, S(O)=HCl solution saturated with air, S(Ar)=HCl solution saturated with argon. The ranges of results for approximately 100 electrode measurements under the four sets of experimental conditions respectively are:

- | |
|---|
| (a) $E^\circ = 0.22260$ to 0.22350 V |
| (b) $E^\circ = 0.22250$ to 0.22260 V |
| (c) $E^\circ = 0.22240$ to 0.22250 V |
| (d) $E^\circ = 0.22230$ to 0.22240 V. |

The results indicate that oxygen does have an effect on the E° for the Ag,AgCl electrode, and is most pronounced in those measurements made with electrodes exposed to an oxygen atmosphere. The higher potentials observed for such electrodes are probably due to mixed potentials from electrochemical couples other than silver-silver chloride, silver-silver oxide, for instance. However, the long term stability could not be maintained and the overall reproducibility for each set was only ± 0.05 mV as compared with 0.01 to 0.02 mV as reported in the literature [10,19,25]². Work is continuing

²It was pointed out by Hamer [26] that Harned and his students used "limited" solutions and filled their cells under vacuum to get rid of the "air effect." Harned and Ehlers [27] thus obtained $E^\circ = 0.22239$ int. volts. On the present scale this becomes 0.22247 V which is in good agreement with conditions (c).

in the areas of oxygen adsorption and desorption measurements to determine quantitatively the effects of oxygen on E° . This work is necessary to lower the uncertainties in existing pH measurements.

In the second project, work is proceeding to develop matrix-specific pH standards to augment the primary buffer standards currently available. The major reason for these new standards is to take into account residual liquid junction potentials and to minimize their effect. It has been shown conclusively that these effects can seriously bias pH readings, especially if the ionic strengths of the standards and the test solutions are significantly different [22].

Research is now underway to test the feasibility of providing matrix-specific pH standards for selected applications, focusing initially on low ionic strength solutions such as acidic precipitation in the environment.

Recently an interlaboratory test was conducted to test the efficiency of using dilute solutions of a strong acid as working standards for pH measurements in acidic precipitation. The results of this test confirm the problems with residual liquid junction potentials and indicate that the strong acid standards (specific for this application) greatly minimize the problem. It is anticipated that in late 1984 NBS will issue a Research Material (RM) which will incorporate these findings and represent the first attempt at matrix-specific pH standards. The effort will be expanded to include matrices such as seawater, biological fluids, and eventually, non-aqueous media. This new generation of pH standards will be consistent with the current NBS pH scale and will be as thermodynamically meaningful as possible. This should avoid the confusion that would be caused by several inconsistent pH scales.

The ultimate goal of the NBS research program on pH is to develop and maintain a unified pH scale based on clearly stated thermodynamic criteria, with a wide range of applicability to practical pH measurements. The present projects form the foundation for this goal and will lead to intensive investigations into activity coefficients and the concept of single ion activities.

References

- [1] Sorensen, S. P. L., *Comp. Rend. Lab. Carlsberg* **8**, 1 (1909).
- [2] Hitchcock, D. I., and A. C. Taylor, *J. Am. Chem. Soc.* **59**, 1912 (1937).
- [3] Guggenheim, E. A., *J. Am. Chem. Soc.* **52**, 1315 (1930).
- [4] Henderson, P., *Z. Physik. Chem.* **59**, 118 (1907).
- [5] Plank, M., *Wied. Ann.* **39**, 161 (1890); **40**, 561 (1890).
- [6] Hamer, W. J., and S. F. Acree, *J. Res. Natl. Bur. Stand.* **23**, 647 (1939).
- [7] Debye, P., and E. Hückel, *Physik. Z.* **24**, 185 (1923).
- [8] Hückel, E., *Physik. Z.* **26**, 93 (1925).
- [9] Hamer, W. J., and S. F. Acree, *J. Res. Natl. Bur. Stand.* **32**, 215 (1944).
- [10] Harned, H. S., and B. B. Owen, *The Physical Chemistry of Electrolytic Solutions*, 3d ed., Reinhold Book Corp., New York, 1958.
- [11] Robinson, R. A., and R. H. Stokes, *Electrolyte Solutions*, 2d ed., Butterworths Scientific Publ., London, 1959.
- [12] Bates R. G., *Determination of pH*, John Wiley & Sons, New York, 1973.
- [13] Bates, R. G., and E. A. Guggenheim, *Pure Appl. Chem.* **1**, 163 (1960).
- [14] Hamer, W. J., *Trans. Electrochem. Soc.* **7**, 45 (1937).
- [15] Bates, R. G., W. J. Hamer, G. G. Manov, and S. F. Acree, *J. Res. Natl. Bur. Stand.* **29**, 183 (1942).
- [16] Bates, R. G., *CRC Crit. Rev. Anal. Chem.* **247** (1981).
- [17] Durst, R. A., *Standardization of pH Measurements*, Natl. Bur. Stand. SP260-53, Natl. Bur. Stand., 1975.
- [18] Bates, R. G., *Pure Appl. Chem.* **50**, 1701 (1978).
- [19] Ives, D. J. G. and G. Janz, eds. *Reference Electrodes*, Academic Press, New York, 1961.
- [20] Clark, W. M., *The Determination of Hydrogen Ions*, 3d ed. Williams and Wilkins Co., Baltimore, 1928.
- [21] MacInnes, D. A., *The Principles of Electrochemistry*, Reinhold Publ. Corp., New York (1939).
- [22] Koch, W. F., and G. Marinenko, *ASTM Special Technical Publication* 823, 10-17 (1981).
- [23] Illingworth, J. A., *Biochem. J.* **195**, 259-262 (1981).
- [24] Bates, R. G.; E. A. Guggenheim, H. S. Harned, D. J. G. Ives, G. J. Janz, C. B. Monk, R. A. Robinson, R. H. Stokes, and W. F. K. Wynne-Jones, *J. Chem. Physics.* **25**, 361 (1956).
- [25] Bates, R. G., and V. E. Bower, *J. Res. Natl. Bur. Stand.* **53**, 283 (1954).
- [26] Hamer, W. J., private communications.
- [27] Harned, H. S., and R. W. Ehlers, *J. Am. Chem. Soc.* **54**, 1350 (1932).